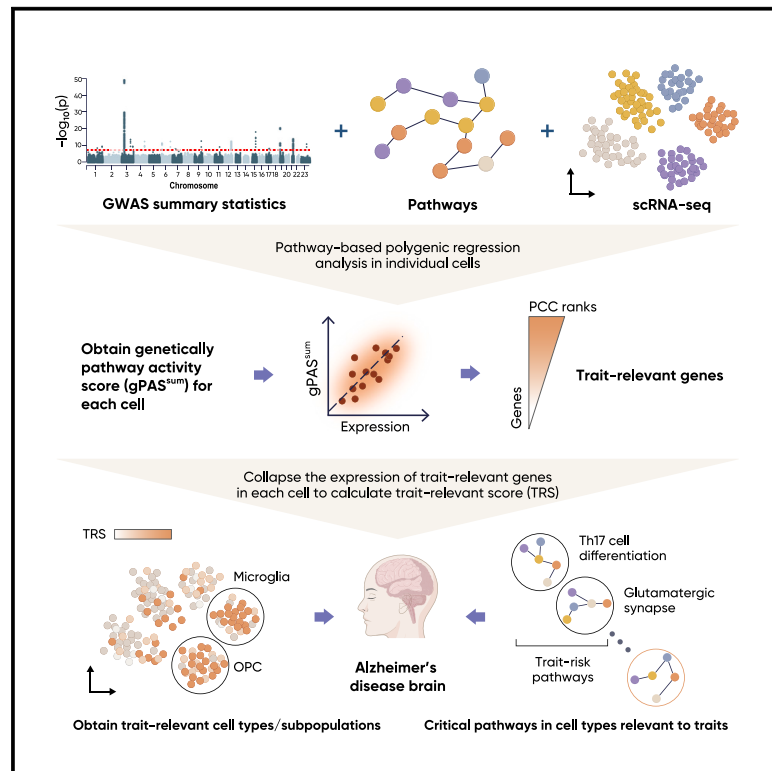


Polygenic regression uncovers trait-relevant cellular contexts through pathway activation transformation of single-cell RNA sequencing data

Graphical abstract



Authors

Yunlong Ma, Chunyu Deng, Yijun Zhou, ..., Yan Zhang, Jian Yang, Jianzhong Su

Correspondence

zhangtyo@hit.edu.cn (Y.Z.),
jian.yang@westlake.edu.cn (J.Y.),
sujz@wmu.edu.cn (J.S.)

In brief

Ma et al. developed scPagwas, a method that integrates coordinated transcriptional features in biological pathways from scRNA-seq data and GWAS summary statistics to prioritize trait-relevant genes and cell subpopulations. Using scPagwas, they recapitulate well-known cell-type-disease associations and identify novel critical cell populations by which genetic variants influence diseases.

Highlights

- Polygenic regression of scRNA-seq and GWAS enhances trait-relevant gene discovery
- scPagwas pinpoints trait-relevant cell subpopulations and states
- scPagwas uncovers specific pathways in cell subpopulations relevant to traits
- Novel insights into the cellular genetic mechanisms underlying complex diseases



Article

Polygenic regression uncovers trait-relevant cellular contexts through pathway activation transformation of single-cell RNA sequencing data

Yunlong Ma,^{1,2,6} Chunyu Deng,^{3,6} Yijun Zhou,^{1,2,6} Yaru Zhang,^{1,2} Fei Qiu,¹ Dingping Jiang,¹ Gongwei Zheng,¹ Jingjing Li,¹ Jianwei Shuai,² Yan Zhang,^{3,*} Jian Yang,^{4,5,*} and Jianzhong Su^{1,2,7,*}

¹School of Biomedical Engineering, School of Ophthalmology & Optometry and Eye Hospital, Wenzhou Medical University, Wenzhou, Zhejiang 325027, China

²Oujiang Laboratory, Zhejiang Lab for Regenerative Medicine, Vision and Brain Health, Wenzhou, Zhejiang 325101, China

³School of Life Science and Technology, Harbin Institute of Technology, Harbin, Heilongjiang 150080, China

⁴School of Life Sciences, Westlake University, Hangzhou, Zhejiang 310012, China

⁵Westlake Laboratory of Life Sciences and Biomedicine, Hangzhou, Zhejiang 310024, China

⁶These authors contributed equally

⁷Lead contact

*Correspondence: zhangtyo@hit.edu.cn (Y.Z.), jian.yang@westlake.edu.cn (J.Y.), sujz@wmu.edu.cn (J.S.)

<https://doi.org/10.1016/j.xgen.2023.100383>

SUMMARY

Advances in single-cell RNA sequencing (scRNA-seq) techniques have accelerated functional interpretation of disease-associated variants discovered from genome-wide association studies (GWASs). However, identification of trait-relevant cell populations is often impeded by inherent technical noise and high sparsity in scRNA-seq data. Here, we developed scPagwas, a computational approach that uncovers trait-relevant cellular context by integrating pathway activation transformation of scRNA-seq data and GWAS summary statistics. scPagwas effectively prioritizes trait-relevant genes, which facilitates identification of trait-relevant cell types/populations with high accuracy in extensive simulated and real datasets. Cellular-level association results identified a novel subpopulation of naive CD8⁺ T cells related to COVID-19 severity and oligodendrocyte progenitor cell and microglia subsets with critical pathways by which genetic variants influence Alzheimer's disease. Overall, our approach provides new insights for the discovery of trait-relevant cell types and improves the mechanistic understanding of disease variants from a pathway perspective.

INTRODUCTION

Genome-wide association study (GWAS) data on complex diseases and numerous genotype-phenotype associations have tremendously accumulated in the past decades.^{1–4} However, functional interpretation of these variants identified by GWASs remains challenging. It is still unclear how these variants regulate key biological pathways in relevant tissues/cell types to mediate disease development. The advent of single-cell RNA sequencing (scRNA-seq) technology has provided an unprecedented opportunity to characterize cell populations and states from heterogeneous tissues.^{5,6} Unveiling trait-relevant cell populations from scRNA-seq data is crucial for exploring the mechanistic etiology of complex traits (including diseases).⁷ Thus, linking scRNA-seq data with genotype-phenotype association information from GWASs has considerable potential to provide new insights into the polygenic architecture of complex traits at a high resolution.^{8–12}

Several studies have revealed significant enrichment of complex traits in relevant tissue types by integrating tissue-specific gene expression profiles with GWAS summary statistics.^{13–15}

Inspired by these tissue-type enrichment methods, several methods,^{16–21} including LDSC-SEG, RolyPoly, and MAGMA-based approaches, have been employed to incorporate GWAS and scRNA-seq data to identify predefined cell types associated with complex traits. However, these approaches largely neglect the considerable heterogeneity within each cell type and thus are not suitable for making inferences at single-cell resolution. Recently, scDRS²² was developed to distinguish disease-associated cell populations at the single-cell level; however, its accuracy relies heavily on a set of disease-specific genes identified from GWAS data using gene-based association test methods,^{23–26} such as MAGMA.²⁶ Although the gene-scoring methods focus on the top significant genotype-phenotype associations and have been applied to bulk tissue or aggregated data analysis, it is still challenging to use these methods to make accurate per-cell-based inferences in scRNA-seq data. The top genetic association signals at specific loci may be absent from most cells because of the extensive sparsity and technical noise in single-cell data.^{27,28} To the best of our knowledge, there is no method that simultaneously considers the expression features of single-cell data and polygenic risk signals from GWAS summary



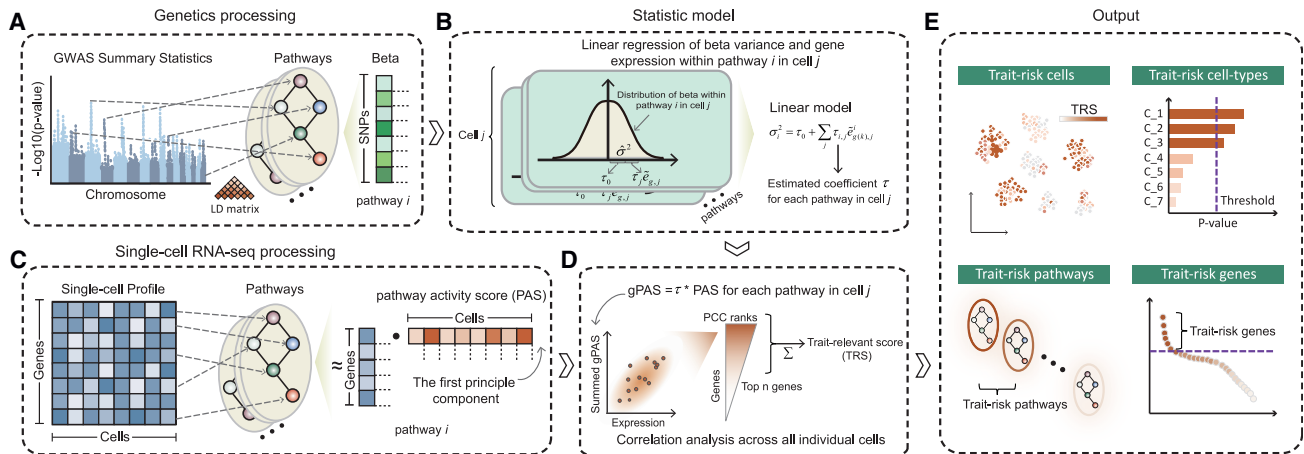


Figure 1. Overview of scPagwas approach

(A) Linking single-nucleotide polymorphisms (SNPs) from GWAS summary statistics into corresponding pathways. The linkage disequilibrium (LD) matrix for SNPs is calculated based on the 1,000 Genomes Project phase 3 panel.

(B) Statistical model. The pathway-based polygenic regression analysis between SNP effect sizes and adjusted gene expression within a given pathway i is used to infer an estimated coefficient τ for each pathway in cell j .

(C) Transforming gene-by-cell matrix to pathway activity score (PAS)-by-cell matrix via using the singular value decomposition (SVD) method. The first principal component (PC1) represents the PAS for pathway i in a given cell j .

(D) The Pearson correlation model. The genetically associated PAS (gPAS) for each pathway is defined as the product between the estimated coefficient τ and the weighted PAS in a given cell j (see STAR Methods). The bottom panel indicates the Pearson correlation analysis of the summed gPASs (gPAS^{sum}) of all pathways in cell j correlating with the expression of a given gene across all individual cells and ranking Pearson correlation coefficients (PCCs) to prioritize top trait-relevant genes. Then, scPagwas uses the cell-scoring method in Seurat to collapse the expression of top n trait-relevant genes (default top 1,000 genes) for calculating the trait-relevant score (TRS) of each cell.

(E) scPagwas outputs. The typical outputs includes (1) trait-relevant cells, (2) trait-relevant cell types, and (3) trait-relevant pathways/genes.

statistics to optimize effective and robust trait-relevant genes for accurate inference of disease-associated cells at a fine-grained resolution.

Dynamic cell activities and states are often caused by the combined actions of interacting genes in a given pathway or biological process.²⁹ Compared with leveraging the expression level of individual genes, pathway activity scoring methods that collapse the functional actions of different genes involved in the same biological pathways can prominently enhance statistical power and biological interpretation for determining particular cellular functions or states.^{27,30–32} Recent studies have shown that such pathway-based scoring methods exhibit a greater reduction of technical and biological confounders of scRNA-seq data.^{33–35} Moreover, multiple lines of evidence have suggested that clinically informative variants associated with complex diseases mainly occur in systems of closely interacting genes, and even variants with weak association signals clustered in the same biological pathway could provide critical information to understand the genetic basis of complex diseases.^{36,37} Thus, integrating coordinated transcriptional features in biological pathways from scRNA-seq data and polygenic risk signals from GWAS summary statistics is a promising approach to prioritize trait-relevant genes and distinguish critical cells by which genetic variants influence diseases.

Here, we present a pathway-based polygenic regression method (scPagwas) that integrates scRNA-seq and GWAS data for the discovery of cellular context critical for complex diseases and traits. scPagwas performs a linear regression of GWAS signals on pathway activation transformed from scRNA-seq data to iden-

tify a set of trait-relevant genes, which are subsequently used to infer the most trait-relevant cell subpopulations. We show that scPagwas outperforms the state-of-the-art methods using extensive simulated and real scRNA-seq datasets. Through scPagwas-based analyses of different diseases, we provide new biological insights into how disease-associated naive CD8⁺ T cells are involved in COVID-19 severity and how subsets of microglia and oligodendrocyte progenitor cells (OPCs) can contribute to Alzheimer's disease (AD) risk.

RESULTS

Overview of scPagwas

Given extensive evidence^{16,18,38,39} indicating a positive correlation between genetic associations for a trait of interest and expression levels of genes in trait-relevant bulk tissue or specific cell type, we apply this principle to scRNA-seq data and take advantage of gene expression signatures shared in a biological pathway. scPagwas first links single-nucleotide polymorphisms (SNPs) in the GWAS summary data to each pathway by annotating SNPs to their proximal genes of the corresponding pathway (Figure 1A). Based on the above assumption inspired by previous studies,^{16,18,38,39} scPagwas adopts a linear regression model to calculate the correlation between the genetic effects of SNPs and the gene expression levels within a given pathway to estimate regression coefficient τ in each cell (Figure 1B). The τ is the per-SNP contribution of one unit of pathway-based gene expression activity to heritability in a given cell, reflecting the strength of association between cell-specific pathway activity levels and the variance of SNP effects.⁴⁰

Meanwhile, scPagwas transforms the normalized gene-by-cell matrix to a pathway activity score (PAS)-by-cell matrix, which is constructed using the first principal component (PC1) of gene expression in each pathway via the singular value decomposition (SVD) method^{28,41} (Figure 1C; see STAR Methods). Unless otherwise specified, scPagwas limits pathways with gene sizes ranging from 5 to 300 in the Kyoto Encyclopedia of Genes and Genomes (KEGG) database⁴² to calculate corresponding PASs in each cell.

Following previous studies,^{18,40} we compute the product of $\hat{\tau}$ and PAS for each pathway, hereinafter referred to as genetically associated PAS (gPAS), to capture cell-specific pathway-based genetic variances for traits of interest in a given cell (Figure 1D). Then, we use the central limit theorem method⁴³ to identify significant trait-relevant pathways based on the ranking of gPASs of pathways across individual cells within each cell type (see STAR Methods). In the meanwhile, we compute the sum of gPASs (denoted as gPAS^{sum}) over all included pathways from the KEGG resource⁴² in each cell, correlate it with the expression level of each gene across cells, and prioritize the trait-relevant genes by ranking the Pearson correlation coefficients (PCCs; Figure 1D). Finally, a trait-relevant score (TRS) of each cell is computed by averaging the expression level of the trait-relevant genes and subtracting the random control cell score via the cell-scoring method used in Seurat⁴⁴ (see STAR Methods). By treating the set of cells in a predefined cell type as a pseudo-bulk transcriptomic profile, scPagwas can also be employed to infer significant trait-relevant cell types using the block bootstrap method.⁴⁵

The input of scPagwas includes gene sets of pathways, a gene-by-cell matrix of scRNA-seq data, and summary statistics from a GWAS or meta-analysis for a quantitative trait or disease (case-control study). The typical output includes (1) per-cell-based TRSs and the corresponding p values, (2) trait-associated cell types from the block bootstrap analysis, (3) trait-relevant pathways based on the ranked gPASs, and (4) trait-relevant genes based on the ranked PCCs (Figure 1E).

scPagwas effectively identifies trait-relevant genes

Because trait-relevant genes are vital for inferring the TRS of each cell, we compared the biological functions of the top 1,000 trait-relevant genes identified from scPagwas with those identified with the widely used gene-scoring method MAGMA²⁶ and three other well-established expression quantitative trait locus (eQTL)-based methods including transcriptome-wide association study (TWAS),²³ S-PrediXcan,²⁵ and S-MultiXcan.²⁴ A panel of 10 highly heritable hematopoietic traits was used for benchmark analysis (Tables S1 and S2). We found that trait-relevant genes identified by scPagwas were more highly enriched in functional gene sets related to blood cell traits than those identified by the other four gene-scoring methods (Figure 2A; Table S3). For example, the lymphocyte count-relevant genes prioritized by scPagwas showed highly significant enrichment in biological processes related to immune response, including T cell activation, adaptive immune response, leukocyte differentiation, and leukocyte cell-cell adhesion, whereas those prioritized by MAGMA lacked enrichment in any functional term (false discovery rate [FDR] < 0.01; Figure 2B). In addition, the results of other nine hematopoietic traits also showed supportive evidence that scPagwas-identified risk genes were enriched in biological processes relevant to the trait

of interest (Figures S1 and S2; Table S4). The number of significant biological processes enriched by the scPagwas-identified top 1,000 risk genes is highly positively correlated with the precision of scPagwas ($r = 0.88$ and $p = 2.73 \times 10^{-33}$; Figure S3).

In scRNA-seq data, the sparsity and technical noise of individual genes can lead to high computational costs and inadequate association inference at the single-cell level.^{27,28} Using five distinct scRNA-seq datasets, we found that the use of pathway information with scPagwas could remarkably reduce the sparsity compared with that of individual gene-based evaluations (Figure S4). The average expression magnitudes of individual genes showed a strong positive correlation with their variances (Figure 2C, blue line). In contrast, pathway activation scores transformed from transcriptome profiles significantly reduced the technical noise of variances of single-cell data, which facilitated the identification of biologically relevant genes and improved downstream analyses⁴⁶ (Figures 2C and S5). To assess the influence of inaccurate pathway characterization on the robustness of scPagwas, we performed a sensitivity analysis by adding four different proportions of noisy genes (i.e., 5%, 10%, 15%, and 20%) into the KEGG pathways. We observed that the performance of scPagwas remain robust when adding from 5% to 15% noisy genes in pathways, whereas the performance of scPagwas become unstable after adding 20% noisy genes (Figure S6). Furthermore, scPagwas is computationally efficient and scales linearly with the number of cells for both computational cost and memory use (Figure S7). These results demonstrate that scPagwas not only reduces sparsity and technical noise but also prioritizes more biologically relevant genes associated with trait of interest for per-cell-based inference to identify trait-relevant cells.

Assessment of scPagwas in discerning trait-relevant cells

We first assessed the power and precision of scPagwas in identifying trait-relevant cells using a real GWAS dataset and simulated scRNA-seq datasets. We adopted a highly heritable and relatively simple trait, monocyte count, for benchmark analysis, with the GWAS summary statistics from a large-scale study ($N = 563,946$; Table S1). We synthesized a scRNA-seq dataset from fluorescence-activated cell-sorted bulk hematopoietic populations as the ground truth (see STAR Methods), which contained a known relevant cell type (monocytes, $n = 1,000$ cells) and non-relevant cell types (T and B cells, dendritic cells [DCs], and natural killer [NK] cells, $n = 1,000$ cells in total; Figure 3A). We found that scPagwas (using the cell-scoring method of Seurat⁴⁴ by default) could accurately distinguish monocyte count-relevant cells from all simulated cells (precision = 95.9%; Figure 3B). We further examined whether the scPagwas-identified trait-relevant genes could improve the power of the latest cell-scoring method, scDRS,²² by comparing the results with those using the default gene-based method MAGMA. The precision of scDRS in identifying the trait-relevant cells increased from 0.940 when using the the top 1,000 genes prioritized by MAGMA to 0.957 when using the top 1,000 genes prioritized by scPagwas (Figures 3C and 3D).

Moreover, compared with the gene-based methods that incorporate eQTL information (i.e., S-MultiXcan, S-PrediXcan, and TWAS), the scPagwas-identified trait-relevant genes considerably enhanced the performance of the scDRS in distinguishing cells

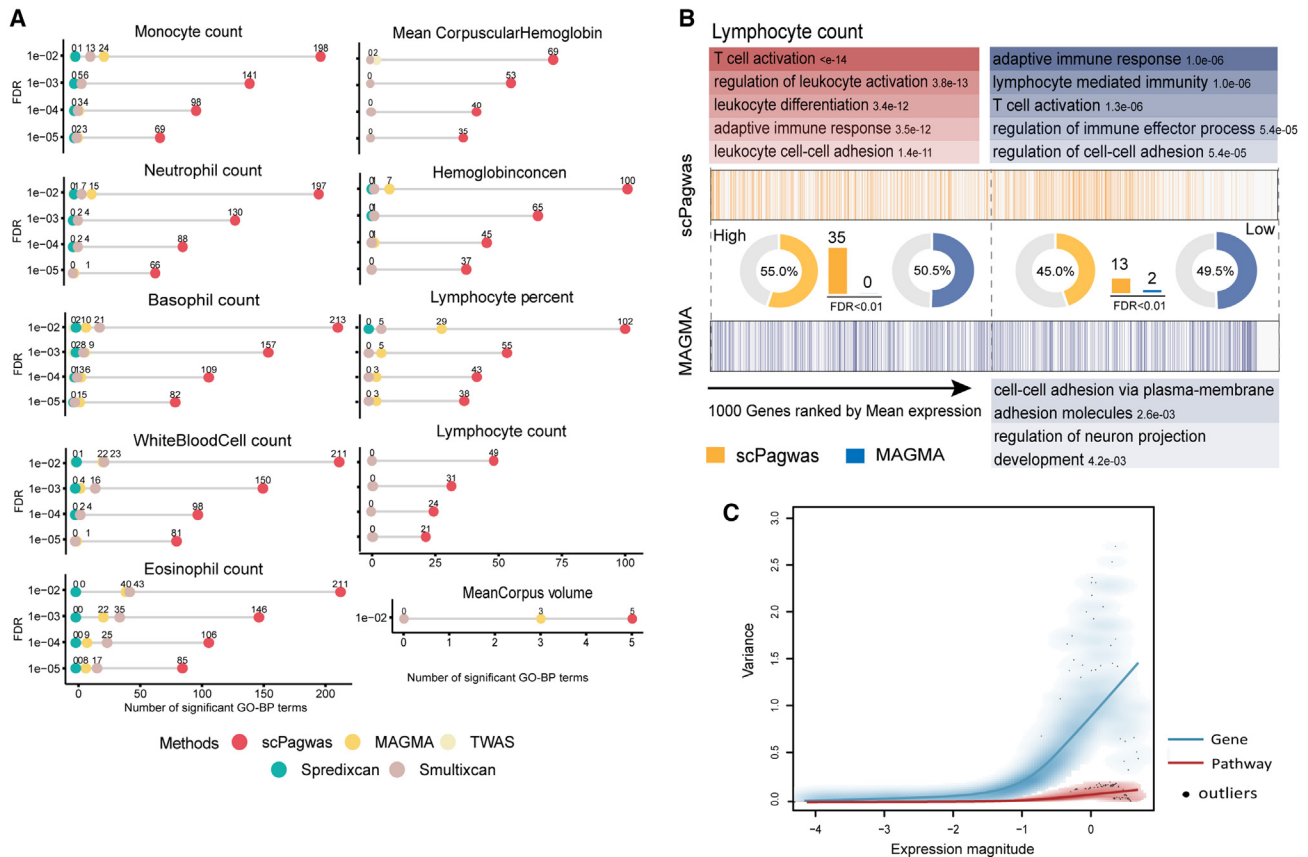


Figure 2. The reproducible and functional results of scPagwas

(A) GO-term enrichment analyses of top-ranked 1,000 genes from scPagwas and other four gene-based methods (i.e., MAGMA, TWAS, S-PrediXcan, and S-MultiXcan) for 10 highly heritable blood cell traits. Different color dots represent number of significant GO terms of biological processes (BPs; FDR <math><0.01</math>) enriched by top-ranked genes from scPagwas and other four methods (see Table S3).

(B) Example of the distribution of scPagwas-identified risk genes and MAGMA-identified risk genes among all genes ranked by their average expression across all cells for the lymphocyte count trait. From left to right in each plot, all genes are ranked by their average expression across all cells. The orange bar indicates each gene in the scPagwas-identified top 1,000 risk genes, and the blue bar indicates each gene in the MAGMA-identified 1,000 risk genes. The percentages of risk genes for the top-half (over-expression genes) and the bottom-half (down-expression genes) cells are shown in the plot accordingly. GO enrichment results (BP terms) of the lymphocyte count trait classified by two groups of over-expression genes (FDR <math><0.01</math>, 35 significant GO terms enriched by scPagwas vs. 0 GO terms by MAGMA) and down-expression genes (FDR <math><0.01</math>, 13 significant GO terms enriched by scPagwas vs. 2 GO-terms by MAGMA) are shown in the plot.

(C) Plot demonstrating the variance of gene-level expression magnitude and pathway-level expression magnitude in the BMMC scRNA-seq dataset ($n = 35,582$ cells). Fitted line with red color represents pathway-level expression magnitude, which shows a mean-variance fit that demonstrates the relationship between average expression of genes in a given pathway (x axis) and its corresponding variance (y axis). Fitted line with blue color represents gene-level expression magnitude, which shows a mean-variance fit that demonstrates the relationship between average gene expression (x axis) and gene variance (y axis). The black dots in the plot indicate outliers.

See also Figure S5.

relevant to the monocyte count trait (scPagwas precision = 95.7% vs. the other three methods' precision = 62.9%–90%; Figure S8A). Using the same simulated single-cell dataset, we further examined the lymphocyte count trait also with a large-scale GWAS dataset ($N = 171,643$ samples) to benchmark the performance of scPagwas against the other four gene-based methods when using scDRS to score cells. We observed a consistent result that scPagwas yielded the best performance (scPagwas precision = 81.8% vs. the other four methods' precision <math><50\%</math>; Figure S9A). Notably, by applying a Monte Carlo (MC) method to distinguish significant trait-relevant cells, scPagwas identified that monocyte cells with higher TRSs were prone to be significantly associated with mono-

cyte count trait, and other non-monocyte cells with lower TRSs showed non-significant associations (Figure S10A). At the cell-type-level inference, we consistently found that monocyte cell type exhibited significant association with monocyte count trait (Figure S10B). In addition, we evaluated the performance of scPagwas in identifying predefined cell types related to a trait of interest in simulated data. We observed that scPagwas could effectively identify trait-relevant cell types under different genetic architectures when the number of included pathways was more than 100 (Figures S11 and S12).

Next, we assessed whether scPagwas could distinguish monocyte count trait-related enrichment in a real ground-truth

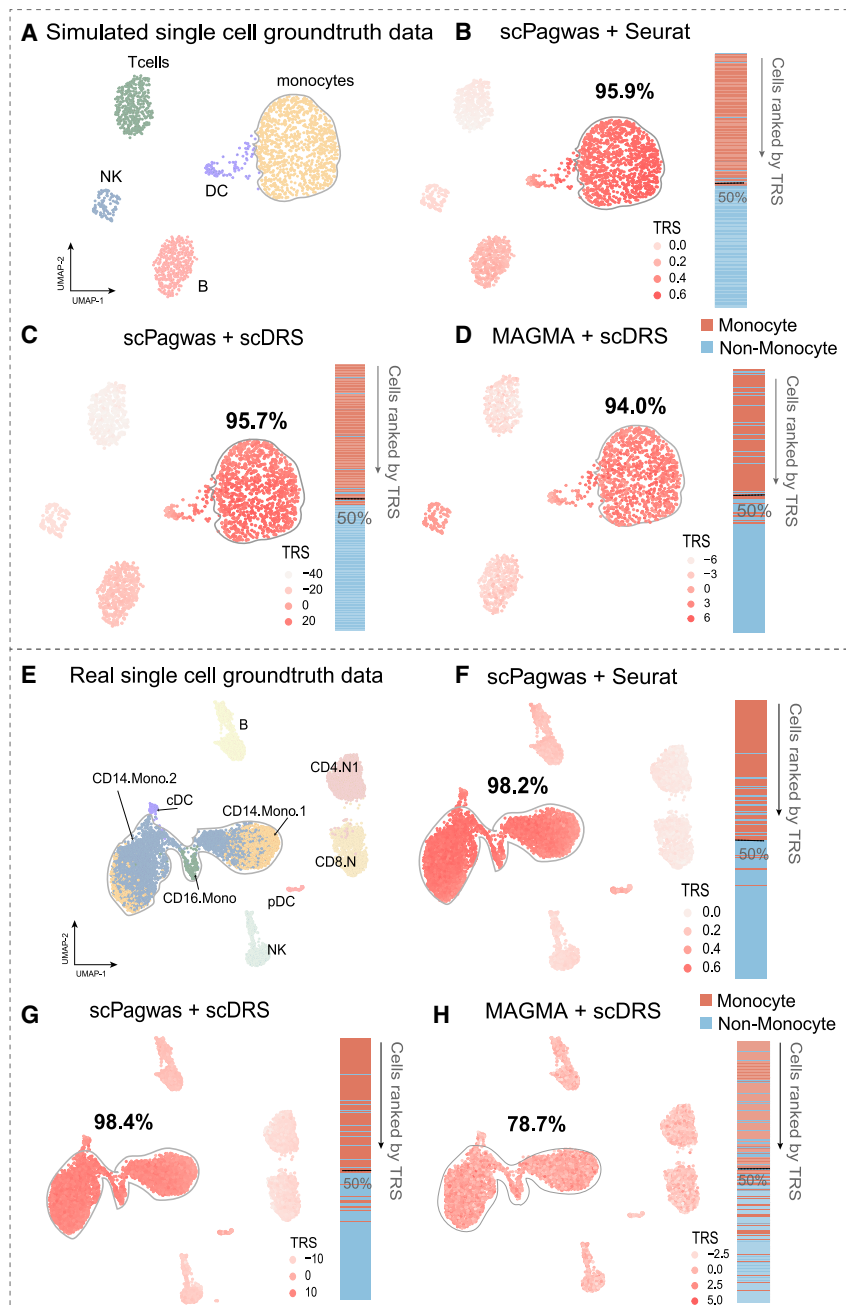


Figure 3. Assessment of the performance of scPagwas in both simulated and real scRNA-seq datasets

(A) Uniform manifold approximation and projection (UMAP) embedding plot shows the cellular component of a synthesized ground-truth scRNA-seq dataset (monocytes: $n = 1,000$ cells, and T, B, DC, and NK: $n = 1,000$ cells in total).

(B) Illustration of the performance of top 1,000 scPagwas-identified genes for identifying monocyte count trait-relevant cells based on the cell-scoring method of Seurat in the synthesized scRNA-seq dataset.

(C) Illustration of the performance of top 1,000 scPagwas-identified genes for identifying monocyte count trait-relevant cells based on scDRS in the synthesized scRNA-seq dataset.

(D) Illustration of the performance of top 1,000 putative disease genes identified by MAGMA for identifying monocyte count trait-relevant cells based on scDRS in the synthesized scRNA-seq dataset.

(E) UMAP plot shows the cellular component of a real ground-truth scRNA-seq dataset. The real BMMC scRNA-seq dataset contains 10,000 cells with seven cell types: monocytes (11_CD14.Mono.1, 12_CD14.Mono.2, and 13_CD16.Mono, $n = 5,000$ cells), DC (09_pDC and 10_cDC, $n = 200$ cells), T cells (19_CD8.N and 20_CD4.N1, $n = 3,000$ cells), B cells (17_B, $n = 1,000$ cells), and NK cells (25_NK, $n = 800$ cells).

(F and G) Illustration of the performance of top 1,000 scPagwas-identified genes for identifying monocyte count trait-relevant cells based on Seurat (F) and scDRS (G) in the real scRNA-seq datasets.

(H) Illustration of the performance of top-ranked 1,000 putative disease genes identified by MAGMA for identifying monocyte count trait-relevant cells based on scDRS in the real scRNA-seq dataset. The UMAP projections of every cell colored by its TRS. The vertical bar exhibits cells descendingly ranked according to their corresponding TRSs (top-ranked 1,000 genes), where red color indicates monocyte cells and blue color indicates non-monocyte cells. The accuracy of each method represents the percentage of monocyte count trait-related cells (i.e., monocytes) for the top-half cells that are ranked by TRS for all cells in a descending manner.

See also [Figures S8–S10](#).

scRNA-seq dataset (Figure 3E) that contained monocytes (CD14⁺ and CD16⁺ monocytes, $n = 5,000$ cells) and non-monocyte cells (T cells [$n = 3,000$], B cells [$n = 1,000$], DCs [$n = 200$], and NK cells [$n = 800$]) from a bone marrow mononuclear cell (BMMC) scRNA-seq dataset (Table S2).⁴⁷ Consistent with the simulation results, scPagwas robustly identified the known trait-relevant cell populations with higher precision using Seurat as the cell-scoring method (precision = 98.2%; Figure 3F). Compared with the default setting of scDRS that uses the top 1,000 MAGMA-identified genes, applying the top 1,000 scPagwas-identified genes to scDRS considerably enhanced the dis-

covery of monocyte count-relevant cells with the improvement of the precision from 0.787 to 0.984 (Figures 3G and 3H).

Analogous to the simulation results, we only found a moderate enrichment of monocyte count-relevant cells by applying the top genes prioritized by the three eQTL-based methods (S-MultiXcan, S-PrediXcan, and TWAS) to scDRS analysis (precision = 61.7–71%; Figure S8B). This observation remained reproducible for lymphocyte count with the inclusion of the same real ground-truth scRNA-seq dataset (Figure S9B). When further evaluating whether the number of included top trait-relevant genes influences the power of scoring trait-relevant cells, scPagwas using

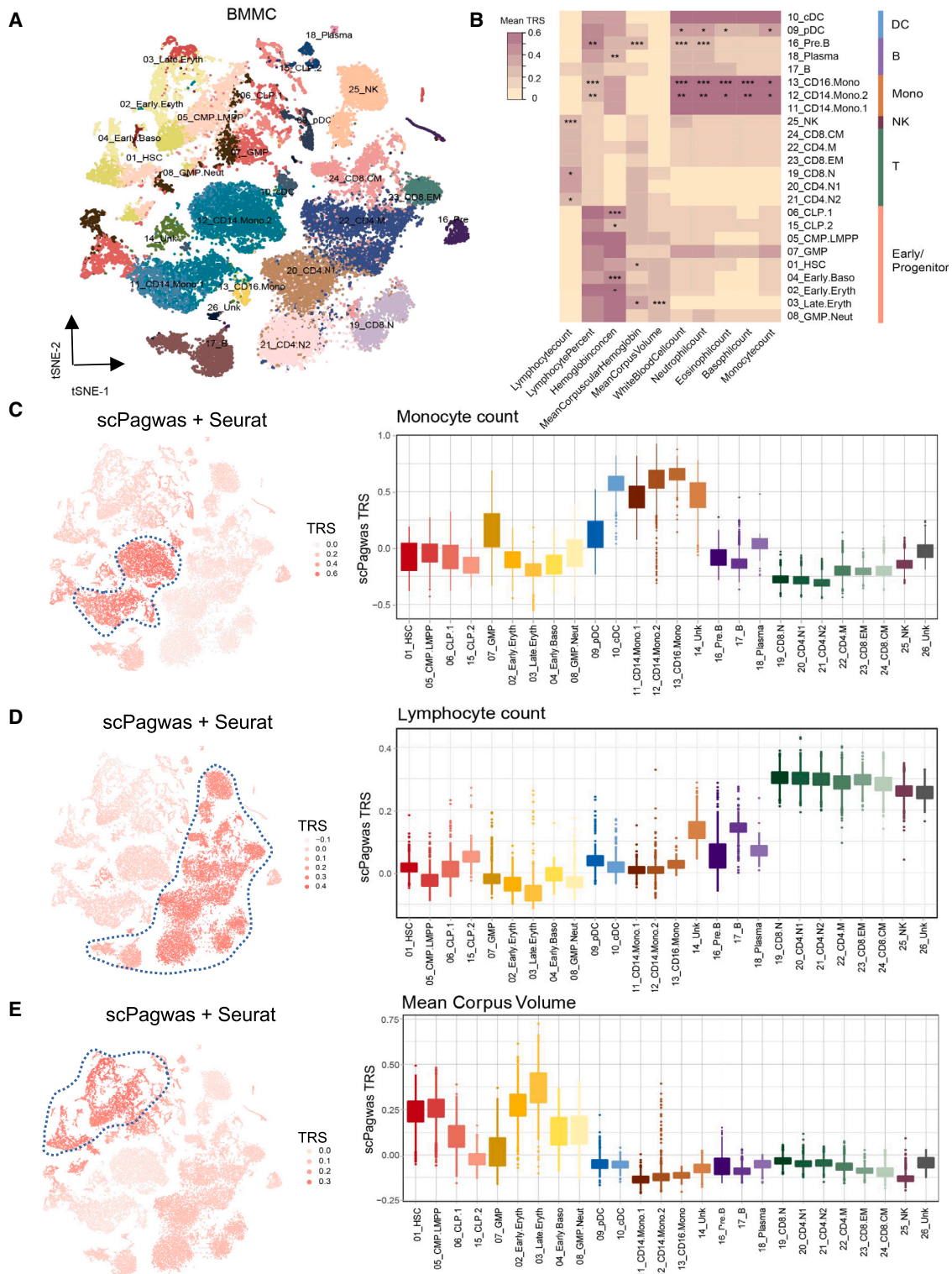


Figure 4. Application of scPagwas to multiple blood cell traits for identifying trait-relevant cells

The 10 hematological traits were analyzed using scPagwas (Seurat) on a large BMMC scRNA-seq dataset.

(A) The tSNE plot shows the cell type labels.

(B) The average TRSs for cells belonging to the same cell type are shown in the heatmap. Unsupervised clustering analysis was conducted, and cell-type categories were grouped into six main clusters, including DCs, B cells, monocytes (Monos), NKs, T cells, and early/progenitor cells. cDC, classical dendritic cell;

(legend continued on next page)

the scDRS method achieved a stable and robust performance after choosing the top 100 trait-relevant genes. In contrast, the use of scDRS with MAGMA resulted in a variable and moderate performance that was largely influenced by the number of included genes prioritized by MAGMA or the three other eQTL-based methods (Figures S13A and S13B).

Additionally, when applying genes prioritized by scPagwas to two other cell-scoring methods, e.g., VISION³⁵ and AUCell,³³ we consistently found that these cell-scoring methods yielded a high performance in identifying cells relevant to monocyte count with either the simulated or the real RNA-seq data (Figures S8C and S8D). Recently, there have been two novel methods, sc-linker⁹ and EPIC,²¹ for inferring trait-relevant cell types. By benchmarking with these two methods at the cell-type level, we detected that scPagwas outperformed both sc-linker and EPIC for identifying monocyte count trait-relevant cell types in simulated and real data (Figures S14A and S14B; Tables S5 and S6). Taken together, our results reveal that scPagwas enables trait relevance to be accurately and robustly characterized at the single-cell resolution.

scPagwas accurately identifies blood cell trait-relevant cell populations at distinct stages of human hematopoiesis

scPagwas was used to identify hematological trait-relevant cell populations in a large BMMC scRNA-seq dataset ($n = 35,582$ cells; Figure 4A) that contained the full spectrum of human hematopoietic differentiation from stem cells to their progeny.⁴⁷ To explore the genetic associations for 10 highly heritable blood cell traits in various cellular contexts, we aggregated the TRSs of individual cells within the same annotated cell type to assess the enrichments of hematopoietic traits at distinct stages of human hematopoiesis using the unsupervised clustering method (Table S1). According to the aggregation results, different cell populations from the same lineage were predisposed to have consistent associations across relevant traits (Figures 4B and S15A; Table S7). For example, red blood cell traits, including hemoglobin concentration, mean corpuscular hemoglobin, and mean corpus volume, tended to have similar associations within the same module based on the TRS of the cell type, consistent with previous findings.²⁸

The TRSs of cells for three representative traits are shown in low-dimensional t-distributed stochastic neighbor embedding (t-SNE) space (Figures 4C–4E). Remarkably, cell lineages relevant to corresponding blood cell traits yielded considerably high TRSs under different conditions (Figures 4C–4E and S15B–S15D), indicating that the cell specificity of these genetic effects was well captured by scPagwas. For monocyte count, scPagwas identified not only monocyte-related cell compart-

ments with increased TRSs but also granulocyte-monocyte progenitor cells showing increased enrichment (Figure 4C). Furthermore, several cell compartments related to CD8⁺ T cells, CD4⁺ T cells, NK cells, and B cells yielded increased TRSs for lymphocyte count (Figure 4D), and early and late erythrocytes, common myeloid progenitor lymphoid-primed multi-potential progenitor (CMP-LMMP), and hematopoietic stem cells exhibited increased TRSs for the mean corpus volume (Figure 4E).

When applying the top 1,000 scPagwas-prioritized genes to scDRS in the BMMC scRNA-seq dataset, cells relevant to three representative traits were enriched and had increased TRSs (Figures S9A–S9C, left panel). However, the use of scDRS with the top 1,000 MAGMA-prioritized genes did not show such trait-relevant enrichment (Figures S16A–S16C, right panel). In an independent peripheral blood mononuclear cell (PBMC) scRNA-seq dataset with a larger number of cells ($n = 97,039$ cells),⁴⁸ consistently, scPagwas using either cell-scoring method, Seurat or scDRS, accurately distinguished monocyte and lymphocyte count-relevant cell compartments, whereas there was no specific trait relevance using scDRS with the top MAGMA-prioritized genes (Figures S17 and S18). Collectively, these results suggest that scPagwas can recapitulate known associations between blood cell traits and the cellular context and identify novel trait-associated cell subpopulations and states.

scPagwas identifies novel immune subpopulations associated with severe COVID-19 risk

Understanding the effects of host genetic factors on immune responses to severe infection can contribute to the development of effective vaccines and therapeutics to control the COVID-19 pandemic.^{49,50} scPagwas was applied to discern COVID-19-associated immune cell types/subpopulations by integrating a large-scale GWAS summary dataset on severe COVID-19 ($N = 7,885$ cases and 961,804 controls) with a large PBMC scRNA-seq dataset ($n = 469,453$ cells) containing healthy controls and patients with COVID-19 with various clinical severities (Tables S1 and S2). scPagwas identified that three immune cell types, including naive CD8⁺ T cells ($p = 4.6 \times 10^{-17}$), megakaryocytes ($p = 7.8 \times 10^{-6}$), and CD16⁺ monocytes ($p = 1.14 \times 10^{-4}$), demonstrated significant associations with severe COVID-19 ($FDR < 0.05$; Figures 5A–5D; Table S8), whereas these three cell types only showed suggestive associations inferred by the three cell-type-level inference methods (LDSC-SEG,¹⁶ MAGMA-based approach,⁵¹ and RolyPoly¹⁸). Both CD16⁺ monocytes and megakaryocytes have been reported to be associated with aggressive cytokine storm among patients with severe COVID-19.^{50,52}

pDC, plasmacytoid dendritic cell; CD4.M, CD4⁺ memory T cells; CD8.CM, CD8⁺ central memory T cells; CD8.EM, CD8⁺ effector memory T cells; CD8.N, CD8⁺ naive T cells; CD4.N1/N2, CD4⁺ naive T cells; CLP, common lymphoid progenitor; CMP, common myeloid progenitor; GMP, granulocyte-macrophage progenitor; LMPP, lymphoid-primed multipotent progenitor; HSC, hematopoietic stem cell; Baso, basophil; Eryth, erythrocyte; Neut, neutrophil. The significant cell type with average TRS ≥ 0.2 is marked with asterisk in the plot (* $FDR < 0.05$, ** $FDR < 0.01$, and *** $FDR < 0.001$).

(C–E) Per-cell TRSs calculated by scPagwas (Seurat) for three representative traits including monocyte count (C), lymphocyte count (D), and mean corpus volume (E) are shown in tSNE coordinates (left) and per cell type (right). Boxplots (left to right: $n = 1,425, 2,260, 903, 377, 2,097, 1,653, 446, 111, 1,050, 544, 325, 1,800, 4,222, 292, 420, 710, 1,711, 62, 1521, 2,470, 2,364, 3,539, 796, 2,080, 2,143$, and 161 cells) show the median with interquartile range (IQR) (25%–75%); whiskers extend 1.5 \times the IQR.

See also Figure S16.

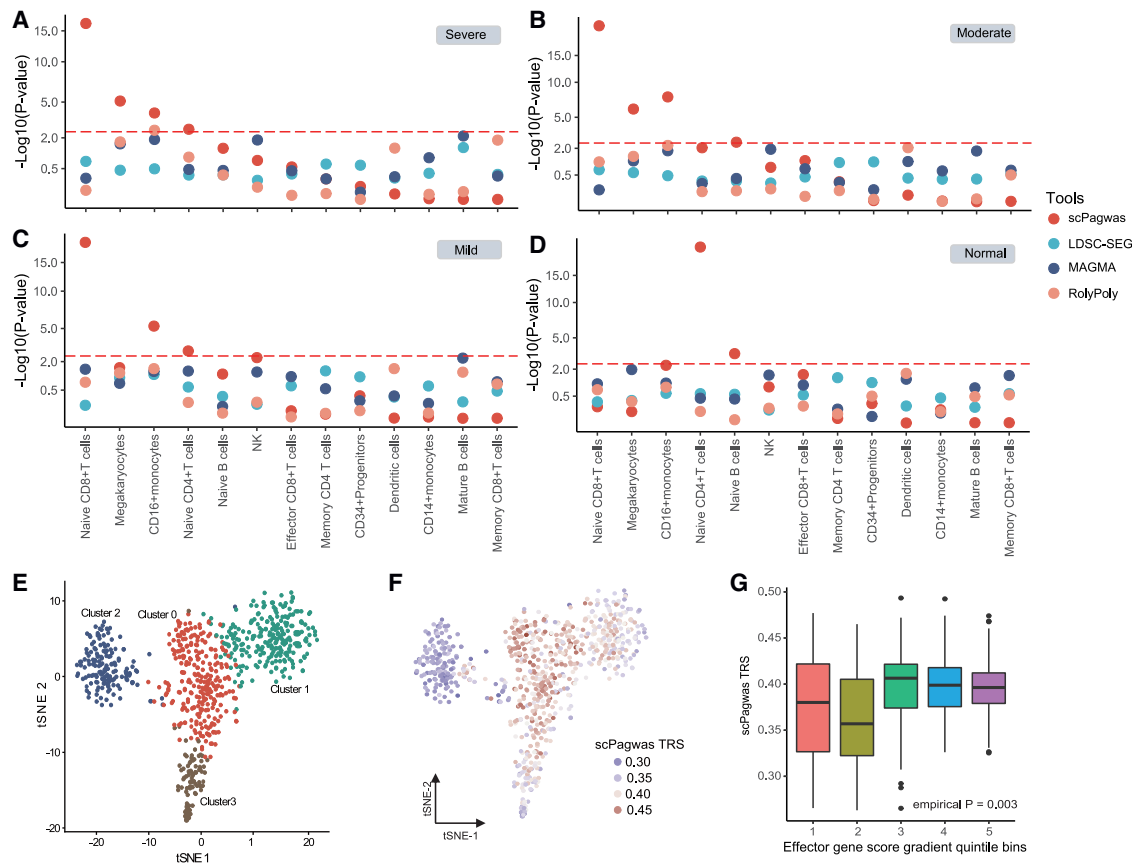


Figure 5. scPagwas identifies trait-relevant immune cell types and subpopulations for severe COVID-19

(A–D) Benchmarking analysis of uncovering trait-relevant cell types by using scPagwas, LDSC-SEG, a MAGMA-based approach, and RolyPoly for patients with COVID-19 with various clinical severities of severe (A), moderate (B), mild (C), and healthy controls (D), respectively. The horizontal red dashed lines represent the significant threshold (Bonferroni-corrected $p < 0.05$).

(E) The tSNE visualization of 766 naive CD8⁺ T cells with four cell clusters.

(F) scPagwas TRS for the phenotype of severe COVID-19 risk is displayed for all naive CD8⁺ T cells in the tSNE plot.

(G) Association between scPagwas TRSs and the molecular signature scores of effector marker genes across all naive CD8⁺ T cells for severe COVID-19. The x axis denotes the gradient quintile bins of effector gene scores across all naive CD8⁺ T cells. The y axis denotes the average scPagwas TRS in each bin for severe COVID-19. The one-sided MC test is used for assessing the statistical significance.

See also [Table S8](#).

Of note, scPagwas identified a novel cell subpopulation of naive CD8⁺ T cells related to severe COVID-19 ([Figures 5A–5E](#)). scPagwas identified that five biological pathways relevant to COVID-19 severities showed high specificity for naive CD8⁺ T cells and included the prolactin signaling pathway, the thyroid hormone signaling pathway, and type 1 diabetes mellitus ($FDR < 0.05$; [Figure S19](#)), which have been reported to potentially play crucial roles in COVID-19.^{53–55} Recent single-cell sequencing studies^{56–58} have demonstrated that naive CD8⁺ T cells show prominent associations with COVID-19 severity. Moreover, naive CD8⁺ T cells are essential for recognizing newly invaded viral antigens including severe acute respiratory syndrome coronavirus 2 (SARS-CoV-2), leading to initiation of the adaptive immune response by differentiating naive T cells into subpopulations of cytotoxic effector CD8⁺ T cells or memory CD8⁺ T cells.^{57,59,60}

As shown in [Figure 5E](#), the naive CD8⁺ T cells were grouped into four clusters. We found that trait-relevant cells with high scPagwas TRSs were mainly in clusters 0 and 1 ([Figures 5F](#)

and [S20](#)). Of note, cluster 0 showed high expression of memory effector marker genes (*GZMK*, *AQP3*, *GZMA*, *PRF1*, and *GNL1*), while cluster 1 demonstrated high expression of exhaustive effector marker genes (*LAG3*, *TIGIT*, *GZMA*, *GZMB*, *PRDM1*, and *IFNG*) ([Figure S21](#)). Further analysis showed that the molecular signature scores of the effector marker genes across cells were significantly positively associated with the TRSs (MC-based empirical $p = 0.003$; [Figure 5G](#); [Table S9](#)), indicating that severe COVID-19-associated T cells tend to activate effector signatures involved in the anti-viral immune response. These new cell subpopulations may play important roles in modulating the immune response in patients with severe COVID-19.

scPagwas distinguishes heterogeneous cell populations associated with AD

AD is a detrimental neurodegenerative disease that causes a gradual increase in neuronal death and loss of cognitive function.

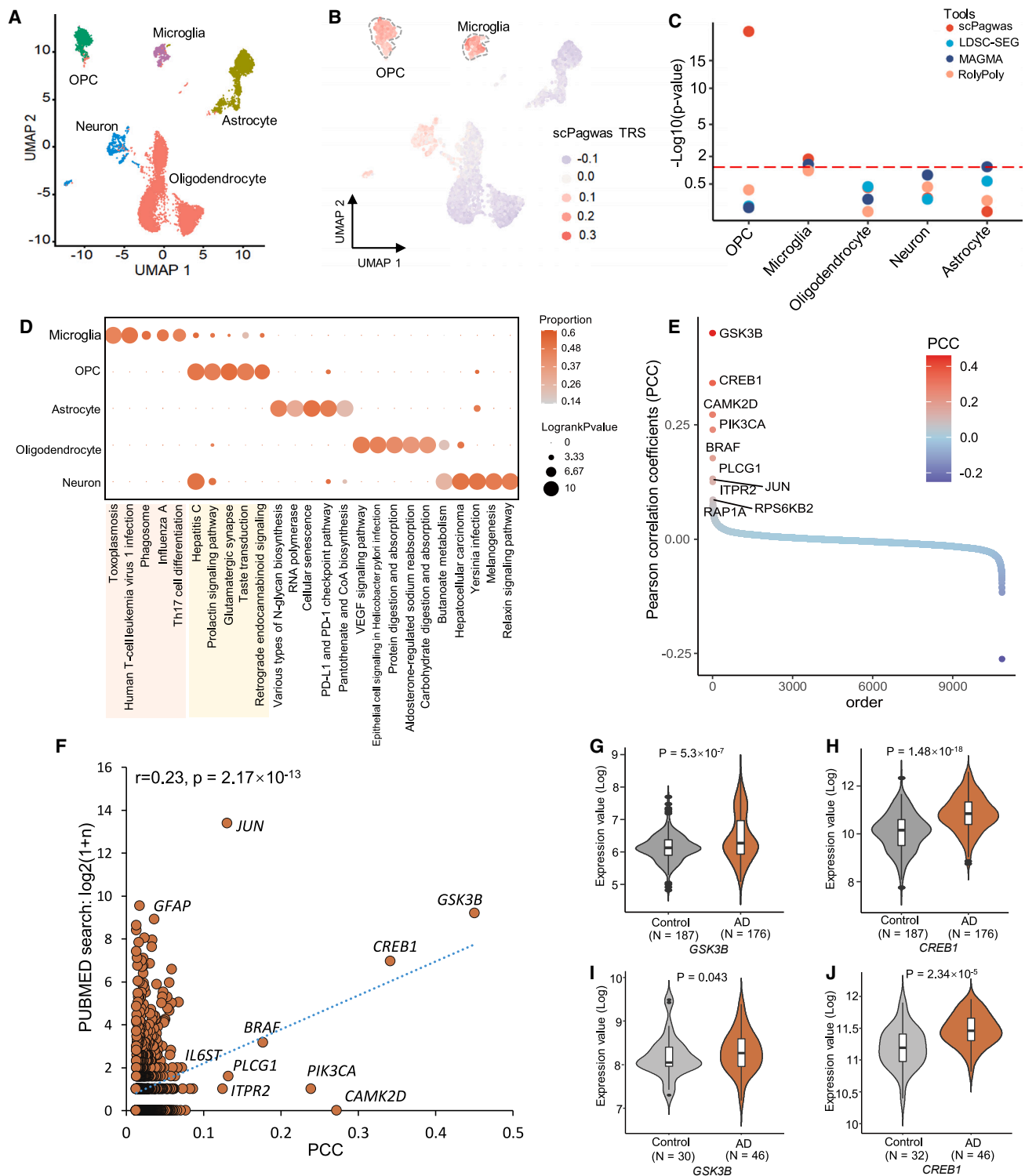


Figure 6. scPagwas discerns human brain cell types and subpopulations in association with AD

(A) The UMAP plot of scRNA-seq profiles of 11,786 human brain cells containing five brain cell types. Cells are colored by the cell-type annotation. (B) scPagwas TRS for the phenotype of AD risk is displayed for all cells in the UMAP plot. OPCs and microglial cells are highlighted with dashed lines. (C) Benchmarking analysis of uncovering significant AD-associated cell types by using scPagwas, LDSC-SEG, a MAGMA-based approach, and RolyPoly. The horizontal red dashed line represents the significant threshold ($p < 0.05$).

(legend continued on next page)

scPagwas was applied to uncover cell subpopulations associated with AD by integrating a human brain entorhinal cortex single-nucleus RNA-seq (snRNA-seq) dataset containing five brain cell types ($n = 11,786$ cells; Figure 6A; Table S2) with an AD GWAS summary dataset ($N = 21,982$ cases and 41,944 controls; Table S1). We found that OPCs and microglia with higher TRSs showed stonger enrichments in AD (Figure 6B). Consistently, at the cell-type level, both OPCs and microglia were significantly associated with AD ($FDR < 0.05$; Figure 6C; Table S10). For independent validation, three large single-cell datasets (Table S1), including two human brain snRNA-seq datasets ($n = 101,906$ and 14,287 cells) and one mouse brain scRNA-seq dataset ($n = 160,796$ cells), were used for scPagwas analysis. These results also indicated that OPCs and microglia were significantly associated with AD ($p < 0.05$; Table S11).

Remarkably, heterogeneous associations between OPCs and AD were detected by scPagwas (heterogeneous $FDR = 3.33 \times 10^{-4}$; Figure S22), which is consistent with the recent finding of functionally diverse states of OPCs.⁶¹ Disruption of OPCs is related to accelerated myelin loss and cognitive decline and is considered an early pathological sign of AD.⁶² Analogous to our results, a recent genetic study⁶³ demonstrated that OPCs exhibit significant associations with schizophrenia, which was repeated by scPagwas using the same schizophrenia GWAS and scRNA-seq data as in the Agarwal et al. study⁶³ (Figure S23). Consistently, multiple lines of genetic evidence have indicated a critical role of microglia in the pathogenesis of AD.^{9,64–66}

Moreover, the top significant trait-relevant pathways of the microglial association were related to immune pathways, including Th17 cell differentiation and influenza A (Figure 6D). Genes in the immune pathway of Th17 cell differentiation in disease-associated microglia have been identified as being involved in AD risk.⁶⁷ The top-ranked significant pathways for OPC associations were related to brain development and synaptic transmitters, including glutamatergic synapses, taste transduction, and the prolactin signaling pathway (Figure 6D). Alteration of glutamatergic synapses has the potential to inhibit OPC proliferation and may be related to disruption of myelination, which is a prominent feature of AD.⁶⁸ These results suggest that these trait-relevant cell types could contribute to AD risk via distinct biological pathways.

We further identified the 1,000 top-ranked trait-relevant genes for AD by computing the correlation between the expression of a given gene and the summed gPASs of each cell across all 11,786 brain cells (see STAR Methods and Figure 6E). To assess the association between these prioritized genes and AD, we adopted the RISmed method,⁶⁹ which searches for supporting evidence from reported studies in the PubMed database. A significant positive correlation was observed between the scPagwas re-

sults and PubMed search results ($r = 0.23$, $p = 2.17 \times 10^{-13}$; Figure 6F), which was notably higher than that from matched random gene sets (permuted $p < 0.01$; Figure S24). These risk genes were significantly enriched in several important functional cellular components related to neurodegenerative diseases, including postsynaptic specialization and neuron-to-neuron synapses ($FDR < 0.05$; Figure S25; Table S12). To further evaluate the phenotypic associations of these top 1,000 scPagwas-identified risk genes, we leveraged two large and independent bulk-based expression profiles on patients with AD ($N = 222$) and matched controls ($N = 219$). We found that 42.1% (421/1,000) of these genes were significantly up-regulated in patients with AD (two-sided t test $p < 0.05$; Table S13). Of note, this proportion was significantly higher than that of randomly selected length-matched genes (permuted $p = 0.01$; Figure S26).

The highest-ranked genes, *CREB1* ($p = 1.48 \times 10^{-18}$ and 2.34×10^{-5}) and *GSK3B* ($p = 5.3 \times 10^{-7}$ and 0.043), exhibited significantly higher expression in patients with AD than in controls in both datasets (Figures 6G–6J). Genetic variants in *CREB1* have been associated with brain-related phenotypes, including neuroticism,⁷⁰ major depressive disorder,⁷¹ and cognitive performance.⁷² Inhibition of *GSK3B* expression decreases microglial migration, inflammation, and inflammation-associated neurotoxicity.⁷³ In addition, activation of the kinase *GSK3B* promotes TAU phosphorylation, which corresponds to amyloid- β ($A\beta$) accumulation and $A\beta$ -mediated neuronal death.⁷⁴ In summary, scPagwas not only identified subpopulations of microglia and OPC relevant to AD but also uncovered the key AD-associated pathways and risk genes.

DISCUSSION

Here, we introduce scPagwas, a pathway-based polygenic regression method that incorporates GWAS summary statistics and scRNA-seq data to identify trait-relevant individual cells. scPagwas exhibits well-calibrated and powerful performance benchmarked with extensive simulated and real datasets. scPagwas can capture the essential trait-relevant features of single-cell data and provide previously unrecognized functional insights by linking trait-relevant genetic signals to the cellular context. It should be noted that scPagwas does not require parameter tuning for cell-type annotations and significantly enhances the discovery of trait-relevant enrichment at the single-cell resolution compared with existing methods.^{16–20} scPagwas is suitable for analyzing genetic enrichment of rare or previously unknown cell populations in large-scale single-cell datasets.

High sparsity and technical noise are the principal issues in analyzing single-cell sequencing data.^{28,30,75–78} The activity of

(D) Dot plot demonstrating the trait-relevant pathways across five brain cell types identified by scPagwas. Dot size represents the log-ranked p value for each pathway, and color intensity indicates the proportion of cells within each cell type genetically influenced by a given pathway (pathway-level coefficient $\beta > 0$).

(E) Trait-relevant genes ranked by the PCCs using scPagwas across all individual cells.

(F) Correlations of trait-relevant genes for AD ranked from scPagwas results and PubMed search results. The Pearson correlation is calculated between scPagwas results and PubMed search results ($\log_2(n + 1)$). The top-ranking trait-relevant genes are labeled.

(G and H) Violin plots show the differential gene expression (DGE) analyses of *GSK3B* and *CREB1* between patients with AD and controls in a GEO: GSE15222 bulk transcriptomic dataset ($n = 176$ patients with AD, and $n = 187$ controls).

(I and J) Violin plots show the DGE of *GSK3B* and *CREB1* between patients with AD and controls in a GEO: GSE109887 bulk dataset ($n = 46$ patients with AD, and $n = 32$ controls). The two-sided Student's t test was used for assessing the statistical significance.

See also Table S13.

individual genes cannot represent cell functionality because it highly relies on the activity of other partner genes in a given pathway.²⁹ Additionally, the combination of biological functions of different genes in the same pathway has been reported to reduce inflated zero counts and technical noise.^{27,30–32,34} Furthermore, disease-associated genetic variants that are mainly involved in systems of highly communicating genes and even variants with weak associations grouped in a given biological pathway could play important roles in uncovering the genetic mechanisms of complex diseases or traits.^{36,37} Leveraging these pathway-based advantages, scPagwas could reduce the high sparsity and technical noise across millions of scRNA-seq profiles from different tissues and organs from mice and humans. Crucially, scPagwas not only recapitulated well-established cell type-disease associations, including the associations of immune cell types with hematological traits and microglia with AD, but also detected notable enrichments that have not been reported in previous studies and are biologically plausible, supporting the powerful potential of scPagwas for the discovery of novel mechanisms.

Based on the correlation between genetically influenced pathway activity and gene expression, scPagwas prioritized more trait-relevant genes than other widely used gene-scoring methods, including MAGMA,²⁶ S-PrediXcan,²⁵ S-MultiXcan,²⁴ and TWAS²³ (Figure 2). Although the use of scDRS with the MAGMA-identified genes was more powerful than with the genes identified by the other three methods (i.e., S-PrediXcan, S-MultiXcan, and TWAS), scPagwas yielded the best performance in distinguishing trait-relevant cells. When the top 1,000 scPagwas-identified trait-relevant genes were applied to scDRS, the precision for distinguishing trait-relevant cells was significantly enhanced, indicating that it is important to prioritize a group of robust trait-relevant genes for scoring cells. This explains why previous cell-scoring methods^{22,33,35} based on the top-ranked MAGMA genes only achieved moderate performance. Most recently, two new methods of sc-linker⁹ and EPIC²¹ have been published to link scRNA-seq data with GWAS summary statistics for identifying trait-relevant cell types. Compared with the disease-specific genes identified from EPIC and gene programs from sc-linker, scPagwas simultaneously leverages the integration of the polygenic risk signals from GWAS summary statistics and the coordinated expression features in biological pathways from single-cell data to prioritize trait-relevant genes, which contribute to distinguish critical trait-relevant cells at a fine-grained resolution. Moreover, scPagwas could discern trait-relevant cell populations as well as early progenitor cells for blood cell traits, which is consistent with the fact that pathway-based scoring methods are useful in determining disease-associated but heterogeneous early developmental progenitor cells.^{34,79,80}

Limitations of the study

Several limitations of this study should be noted. First, identification of a statistical association between complex diseases/traits and individual cells does not imply causality but may reflect indirect identification of causal associations, parallel to previous methods.^{16,18,19,22} Nevertheless, even under such circumstances, the scPagwas-identified trait-relevant cells are inclined

to be biologically relevant to the causal cells because of their similar genetic co-expression patterns. Second, for the current study, we selected canonical pathways identified in the KEGG database⁴² because these pathways have been experimentally validated. Third, to be compatible with Seurat software,⁴⁴ the most extensively used tool for scRNA-seq data analysis, scPagwas by default employed the cell-scoring method of the “Add-ModuleScore” function of Seurat to directly compute the TRS, which makes it convenient to integrate scPagwas into existing scRNA-seq analysis pipelines. According to our current results, other state-of-the-art cell-scoring methods, including the scDRS,²² AUCell,³³ and VISION,³⁵ also showed a good and robust performance for distinguishing trait-relevant cells when applying scPagwas-identified trait-relevant genes. Finally, we annotated SNPs into genes and their corresponding pathways based on the proximal distance of a 20 kb window. It may be possible to establish the link between SNPs and genes using other methods, such as functionally informed SNP-to-gene linking approaches,^{81,82} in the future.

Conclusion

To conclude, scPagwas demonstrates promise for uncovering significant trait-relevant individual cells. Our pathway-based inference strategy will increase the identification of key cell subpopulations with reasonable biological interpretation for traits of interest. From a discovery viewpoint, the identification of reproducible trait-relevant individual cells will help to achieve the first step toward an in-depth experimental investigation of novel cell types or states with potential physiological roles in health and disease.

STAR★METHODS

Detailed methods are provided in the online version of this paper and include the following:

- KEY RESOURCES TABLE
- RESOURCE AVAILABILITY
 - Lead contact
 - Materials availability
 - Data and code availability
- METHOD DETAILS
 - scPagwas methodology
 - Linking SNPs to their corresponding pathways
 - PAS matrix transformation
 - Polygenic regression model
 - Identification of trait-relevant genes and individual cells
 - Inference analysis of trait-relevant cell types
 - Simulations
 - scRNA-seq datasets
 - GWAS summary datasets for complex diseases and traits
- QUANTIFICATION AND STATISTICAL ANALYSIS

SUPPLEMENTAL INFORMATION

Supplemental information can be found online at <https://doi.org/10.1016/j.xgen.2023.100383>.

ACKNOWLEDGMENTS

We acknowledge funding support from the National Natural Science Foundation of China (32200535 to Y.M. and 61871294 and 82172882 to J. Su); the Scientific Research Foundation for Talents of Wenzhou Medical University (KYQD20201001 to Y.M.); the Science Foundation of Zhejiang Province (LR19C060001 to J. Su); the Leading Innovative and Entrepreneur Team Introduction Program of Zhejiang (2021R01013 to J.Y.); the Research Program of Westlake Laboratory of Life Sciences and Biomedicine (202208013 to J.Y.); and Westlake Education Foundation (101566022001 to J.Y.). We thank Dr. Zhenhui Chen from Wenzhou Medical University for providing helpful suggestions and manuscript revisions. We also thank all of the authors who have deposited and shared GWAS summary data in public databases and the authors who publicly released the scRNA-seq and snRNA-seq datasets.

AUTHOR CONTRIBUTIONS

J. Su, J.Y., and Y.M. conceived and designed the study. Y.M., C.D., and Y. Zhou developed the method. Y.M., C.D., Yan Zhang, Yaru Zhang, F.Q., D.J., G.Z., J. Shuai, and J.L. managed data collection. Y.M., C.D., Y. Zhou, Yaru Zhang, and J.L. conducted the bioinformatics analysis and data interpretation. Y.M., J. Su, C.D., Y. Zhou, J.Y., and Yan Zhang wrote the manuscript. All authors reviewed and approved the final manuscript.

DECLARATION OF INTERESTS

The authors declare no competing interests.

Received: February 23, 2023

Revised: May 26, 2023

Accepted: July 25, 2023

Published: August 18, 2023

REFERENCES

- Bycroft, C., Freeman, C., Petkova, D., Band, G., Elliott, L.T., Sharp, K., Motyer, A., Vukcevic, D., Delaneau, O., O'Connell, J., et al. (2018). The UK Biobank resource with deep phenotyping and genomic data. *Nature* 562, 203–209. <https://doi.org/10.1038/s41586-018-0579-z>.
- Ma, Y., Huang, Y., Zhao, S., Yao, Y., Zhang, Y., Qu, J., Wu, N., and Su, J. (2021). Integrative genomics analysis reveals a 21q22. 11 locus contributing risk to COVID-19. *Hum. Mol. Genet.* 30, 1247–1258. <https://doi.org/10.1093/hmg/ddab125>.
- Trubetskoy, V., Pardiñas, A.F., Qi, T., Panagiotaropoulou, G., Awasthi, S., Bigdeli, T.B., Bryois, J., Chen, C.Y., Dennison, C.A., Hall, L.S., et al. (2022). Mapping genomic loci implicates genes and synaptic biology in schizophrenia. *Nature* 604, 502–508. <https://doi.org/10.1038/s41586-022-04434-5>.
- Mallard, T.T., Linnér, R.K., Grotzinger, A.D., Sanchez-Roige, S., Seidnitz, J., Okbay, A., de Vlaming, R., Meddens, S.F.W., Bipolar Disorder Working Group of the Psychiatric Genomics Consortium; and Palmer, A.A., et al. (2022). Multivariate GWAS of psychiatric disorders and their cardinal symptoms reveal two dimensions of cross-cutting genetic liabilities. *Cell Genom.* 2, 100140. <https://doi.org/10.1016/j.xgen.2022.100140>.
- Shapiro, E., Biezuner, T., and Linnarsson, S. (2013). Single-cell sequencing-based technologies will revolutionize whole-organism science. *Nat. Rev. Genet.* 14, 618–630. <https://doi.org/10.1038/nrg3542>.
- Liang, Q., Cheng, X., Wang, J., Owen, L., Shakoor, A., Lillvis, J.L., Zhang, C., Farkas, M., Kim, I.K., Li, Y., et al. (2023). A multi-omics atlas of the human retina at single-cell resolution. *Cell Genom.* 3, 100298. <https://doi.org/10.1016/j.xgen.2023.100298>.
- Hekselman, I., and Yeger-Lotem, E. (2020). Mechanisms of tissue and cell-type specificity in heritable traits and diseases. *Nat. Rev. Genet.* 21, 137–150. <https://doi.org/10.1038/s41576-019-0200-9>.
- Xiang, B., Deng, C., Qiu, F., Li, J., Li, S., Zhang, H., Lin, X., Huang, Y., Zhou, Y., Su, J., et al. (2021). Single Cell Sequencing Analysis Identifies Genetics-Modulated ORMDL3+ Cholangiocytes Having Higher Metabolic Effects On Primary Biliary Cholangitis. *J. Nanobiotechnology* 19, 406. <https://doi.org/10.1186/s12951-021-01154-2>.
- Jagadeesh, K.A., Dey, K.K., Montoro, D.T., Mohan, R., Gazal, S., Engreitz, J.M., Xavier, R.J., Price, A.L., and Regev, A. (2022). Identifying disease-critical cell types and cellular processes by integrating single-cell RNA-sequencing and human genetics. *Nat. Genet.* 54, 1479–1492. <https://doi.org/10.1038/s41588-022-01187-9>.
- Kartha, V.K., Duarte, F.M., Hu, Y., Ma, S., Chew, J.G., Lareau, C.A., Earl, A., Burkett, Z.D., Kohlway, A.S., Lebofsky, R., and Buenrostro, J.D. (2022). Functional inference of gene regulation using single-cell multi-omics. *Cell Genom.* 2, 100166. <https://doi.org/10.1016/j.xgen.2022.100166>.
- Bressan, E., Reed, X., Bansal, V., Hutchins, E., Cobb, M.M., Webb, M.G., Alsop, E., Grenn, F.P., Illarionova, A., Savytska, N., et al. (2023). The Foundational Data Initiative for Parkinson Disease: Enabling efficient translation from genetic maps to mechanism. *Cell Genom.* 3, 100261. <https://doi.org/10.1016/j.xgen.2023.100261>.
- Bossini-Castillo, L., Glinos, D.A., Kunowska, N., Gola, G., Lamikanra, A.A., Spitzer, M., Soskic, B., Cano-Gamez, E., Smyth, D.J., Cattermole, C., et al. (2022). Immune disease variants modulate gene expression in regulatory CD4+ T cells. *Cell Genom.* 2, 100117. <https://doi.org/10.1016/j.xgen.2022.100117>.
- Hu, X., Kim, H., Stahl, E., Plenge, R., Daly, M., and Raychaudhuri, S. (2011). Integrating autoimmune risk loci with gene-expression data identifies specific pathogenic immune cell subsets. *Am. J. Hum. Genet.* 89, 496–506. <https://doi.org/10.1016/j.ajhg.2011.09.002>.
- Pers, T.H., Karjalainen, J.M., Chan, Y., Westra, H.J., Wood, A.R., Yang, J., Lui, J.C., Vedantam, S., Gustafsson, S., Esko, T., et al. (2015). Biological interpretation of genome-wide association studies using predicted gene functions. *Nat. Commun.* 6, 5890. <https://doi.org/10.1038/ncomms6890>.
- Locke, A.E., Kahali, B., Berndt, S.I., Justice, A.E., Pers, T.H., Day, F.R., Powell, C., Vedantam, S., Buchkovich, M.L., Yang, J., et al. (2015). Genetic studies of body mass index yield new insights for obesity biology. *Nature* 518, 197–206. <https://doi.org/10.1038/nature14177>.
- Finucane, H.K., Reshef, Y.A., Anttila, V., Slowikowski, K., Gusev, A., Byrnes, A., Gazal, S., Loh, P.R., Lareau, C., Shores, N., et al. (2018). Heritability enrichment of specifically expressed genes identifies disease-relevant tissues and cell types. *Nat. Genet.* 50, 621–629. <https://doi.org/10.1038/s41588-018-0081-4>.
- Watanabe, K., Taskesen, E., van Bochoven, A., and Posthuma, D. (2017). Functional mapping and annotation of genetic associations with FUMA. *Nat. Commun.* 8, 1826. <https://doi.org/10.1038/s41467-017-01261-5>.
- Calderon, D., Bhaskar, A., Knowles, D.A., Golan, D., Raj, T., Fu, A.Q., and Pritchard, J.K. (2017). Inferring Relevant Cell Types for Complex Traits by Using Single-Cell Gene Expression. *Am. J. Hum. Genet.* 101, 686–699. <https://doi.org/10.1016/j.ajhg.2017.09.009>.
- Watanabe, K., Umičević Mirkov, M., de Leeuw, C.A., van den Heuvel, M.P., and Posthuma, D. (2019). Genetic mapping of cell type specificity for complex traits. *Nat. Commun.* 10, 3222. <https://doi.org/10.1038/s41467-019-11181-1>.
- Skene, N.G., Bryois, J., Bakken, T.E., Breen, G., Crowley, J.J., Gaspar, H.A., Giusti-Rodriguez, P., Hodge, R.D., Miller, J.A., Muñoz-Manchado, A.B., et al. (2018). Genetic identification of brain cell types underlying schizophrenia. *Nat. Genet.* 50, 825–833. <https://doi.org/10.1038/s41588-018-0129-5>.
- Wang, R., Lin, D.-Y., and Jiang, Y. (2022). EPIC: Inferring relevant cell types for complex traits by integrating genome-wide association studies and single-cell RNA sequencing. *PLoS Genet.* 18, e1010251. <https://doi.org/10.1371/journal.pgen.1010251>.
- Zhang, M.J., Hou, K., Dey, K.K., Sakaue, S., Jagadeesh, K.A., Weinand, K., Taychameekitchai, A., Rao, P., Pisco, A.O., Zou, J., et al. (2022). Polygenic enrichment distinguishes disease associations of individual

- cells in single-cell RNA-seq data. *Nat. Genet.* *54*, 1572–1580. <https://doi.org/10.1038/s41588-022-01167-z>.
23. Gusev, A., Ko, A., Shi, H., Bhatia, G., Chung, W., Penninx, B.W.J.H., Janzen, R., de Geus, E.J.C., Boomsma, D.I., Wright, F.A., et al. (2016). Integrative approaches for large-scale transcriptome-wide association studies. *Nat. Genet.* *48*, 245–252. <https://doi.org/10.1038/ng.3506>.
 24. Barbeira, A.N., Pividori, M., Zheng, J., Wheeler, H.E., Nicolae, D.L., and Im, H.K. (2019). Integrating predicted transcriptome from multiple tissues improves association detection. *PLoS Genet.* *15*, e1007889. <https://doi.org/10.1371/journal.pgen.1007889>.
 25. Barbeira, A.N., Dickinson, S.P., Bonazzola, R., Zheng, J., Wheeler, H.E., Torres, J.M., Torstenson, E.S., Shah, K.P., Garcia, T., Edwards, T.L., et al. (2018). Exploring the phenotypic consequences of tissue specific gene expression variation inferred from GWAS summary statistics. *Nat. Commun.* *9*, 1825. <https://doi.org/10.1038/s41467-018-03621-1>.
 26. de Leeuw, C.A., Mooij, J.M., Heskes, T., and Posthuma, D. (2015). MAGMA: generalized gene-set analysis of GWAS data. *PLoS Comput. Biol.* *11*, e1004219. <https://doi.org/10.1371/journal.pcbi.1004219>.
 27. Frost, H.R. (2020). Variance-adjusted Mahalanobis (VAM): a fast and accurate method for cell-specific gene set scoring. *Nucleic Acids Res.* *48*, e94. <https://doi.org/10.1093/nar/gkaa582>.
 28. Yu, F., Cato, L.D., Weng, C., Liggett, L.A., Jeon, S., Xu, K., Chiang, C.W.K., Wiemels, J.L., Weissman, J.S., de Smith, A.J., and Sankaran, V.G. (2022). Variant to function mapping at single-cell resolution through network propagation. *Nat. Biotechnol.* *40*, 1644–1653. <https://doi.org/10.1038/s41587-022-01341-y>.
 29. Schadt, E.E. (2009). Molecular networks as sensors and drivers of common human diseases. *Nature* *461*, 218–223. <https://doi.org/10.1038/nature08454>.
 30. Holland, C.H., Tanevski, J., Perales-Patón, J., Gleixner, J., Kumar, M.P., Mereu, E., Joughin, B.A., Stegle, O., Lauffenburger, D.A., Heyn, H., et al. (2020). Robustness and applicability of transcription factor and pathway analysis tools on single-cell RNA-seq data. *Genome Biol.* *21*, 36. <https://doi.org/10.1186/s13059-020-1949-z>.
 31. Zhang, Y., Ma, Y., Huang, Y., Zhang, Y., Jiang, Q., Zhou, M., and Su, J. (2020). Benchmarking algorithms for pathway activity transformation of single-cell RNA-seq data. *Comput. Struct. Biotechnol. J.* *18*, 2953–2961. <https://doi.org/10.1016/j.csbj.2020.10.007>.
 32. Zhang, Y., Zhang, Y., Hu, J., Zhang, J., Guo, F., Zhou, M., Zhang, G., Yu, F., and Su, J. (2020). scTPA: a web tool for single-cell transcriptome analysis of pathway activation signatures. *Bioinformatics* *36*, 4217–4219. <https://doi.org/10.1093/bioinformatics/btaa532>.
 33. Aibar, S., González-Blas, C.B., Moerman, T., Huynh-Thu, V.A., Imrichova, H., Hulselmans, G., Rambow, F., Marine, J.C., Geurts, P., Aerts, J., et al. (2017). SCENIC: single-cell regulatory network inference and clustering. *Nat. Methods* *14*, 1083–1086. <https://doi.org/10.1038/nmeth.4463>.
 34. Fan, J., Salathia, N., Liu, R., Kaeser, G.E., Yung, Y.C., Herman, J.L., Kaper, F., Fan, J.B., Zhang, K., Chun, J., and Kharchenko, P.V. (2016). Characterizing transcriptional heterogeneity through pathway and gene set overdispersion analysis. *Nat. Methods* *13*, 241–244. <https://doi.org/10.1038/nmeth.3734>.
 35. DeTomaso, D., Jones, M.G., Subramaniam, M., Ashuach, T., Ye, C.J., and Yosef, N. (2019). Functional interpretation of single cell similarity maps. *Nat. Commun.* *10*, 4376. <https://doi.org/10.1038/s41467-019-12235-0>.
 36. Mooney, M.A., Nigg, J.T., McWeeny, S.K., and Wilmot, B. (2014). Functional and genomic context in pathway analysis of GWAS data. *Trends Genet.* *30*, 390–400. <https://doi.org/10.1016/j.tig.2014.07.004>.
 37. Wang, K., Li, M., and Hakonarson, H. (2010). Analysing biological pathways in genome-wide association studies. *Nat. Rev. Genet.* *11*, 843–854. <https://doi.org/10.1038/nrg2884>.
 38. Watanabe, K., Umičević Mirkov, M., de Leeuw, C.A., van den Heuvel, M.P., and Posthuma, D. (2019). Genetic mapping of cell type specificity for complex traits. *Nat. Commun.* *10*, 3222. <https://doi.org/10.1038/s41467-019-11181-1>.
 39. GTEx Consortium; Laboratory Data Analysis & Coordinating Center LDACC—Analysis Working Group; Statistical Methods groups—Analysis Working Group; Enhancing GTEx eGTEx groups; NIH Common Fund; NIH/NCI; NIH/NHGRI; NIH/NIMH; NIH/NIDA; Biospecimen Collection Source Site—NDRI (2017). Genetic effects on gene expression across human tissues. *Nature* *550*, 204–213. <https://doi.org/10.1038/nature24277>.
 40. Gazal, S., Finucane, H.K., Furlotte, N.A., Loh, P.-R., Palamara, P.F., Liu, X., Schoech, A., Bulik-Sullivan, B., Neale, B.M., Gusev, A., and Price, A.L. (2017). Linkage disequilibrium-dependent architecture of human complex traits shows action of negative selection. *Nat. Genet.* *49*, 1421–1427. <https://doi.org/10.1038/ng.3954>.
 41. Tomfohr, J., Lu, J., and Kepler, T.B. (2005). Pathway level analysis of gene expression using singular value decomposition. *BMC Bioinf.* *6*, 225. <https://doi.org/10.1186/1471-2105-6-225>.
 42. Kanehisa, M., and Goto, S. (2000). KEGG: kyoto encyclopedia of genes and genomes. *Nucleic Acids Res.* *28*, 27–30. <https://doi.org/10.1093/nar/28.1.27>.
 43. Rosenblatt, M. (1956). A central limit theorem and a strong mixing condition. *Proc. Natl. Acad. Sci. USA* *42*, 43–47. <https://doi.org/10.1073/pnas.42.1.43>.
 44. Butler, A., Hoffman, P., Smibert, P., Papalexi, E., and Satija, R. (2018). Integrating single-cell transcriptomic data across different conditions, technologies, and species. *Nat. Biotechnol.* *36*, 411–420. <https://doi.org/10.1038/nbt.4096>.
 45. Efron, B., and Tibshirani, R. (1986). Bootstrap methods for standard errors, confidence intervals, and other measures of statistical accuracy. *Stat. Sci.* *1*, 54–75. <https://www.jstor.org/stable/2245500>.
 46. Wu, Y., and Zhang, K. (2020). Tools for the analysis of high-dimensional single-cell RNA sequencing data. *Nat. Rev. Nephrol.* *16*, 408–421. <https://doi.org/10.1038/s41581-020-0262-0>.
 47. Granja, J.M., Klemm, S., McGinnis, L.M., Kathiria, A.S., Mezger, A., Corces, M.R., Parks, B., Gars, E., Liedtke, M., Zheng, G.X.Y., et al. (2019). Single-cell multiomic analysis identifies regulatory programs in mixed-phenotype acute leukemia. *Nat. Biotechnol.* *37*, 1458–1465. <https://doi.org/10.1038/s41587-019-0332-7>.
 48. Stephenson, E., Reynolds, G., Botting, R.A., Calero-Nieto, F.J., Morgan, M.D., Tuong, Z.K., Bach, K., Sungnak, W., Worlock, K.B., Yoshida, M., et al. (2021). Single-cell multi-omics analysis of the immune response in COVID-19. *Nat. Med.* *27*, 904–916. <https://doi.org/10.1038/s41591-021-01329-2>.
 49. Zhang, B., Zhang, Z., Koeken, V.A.C.M., Kumar, S., Aillaud, M., Tsay, H.-C., Liu, Z., Kraft, A.R.M., Soon, C.F., Odak, I., et al. (2023). Altered and allele-specific open chromatin landscape reveals epigenetic and genetic regulators of innate immunity in COVID-19. *Cell Genom.* *3*, 100232. <https://doi.org/10.1016/j.xgen.2022.100232>.
 50. Ma, Y., Qiu, F., Deng, C., Li, J., Huang, Y., Wu, Z., Zhou, Y., Zhang, Y., Xiong, Y., Yao, Y., et al. (2022). Integrating single-cell sequencing data with GWAS summary statistics reveals CD16+ monocytes and memory CD8+ T cells involved in severe COVID-19. *Genome Med.* *14*, 16. <https://doi.org/10.1186/s13073-022-01021-1>.
 51. Bryois, J., Skene, N.G., Hansen, T.F., Kogelman, L.J.A., Watson, H.J., Liu, Z., Eating Disorders Working Group of the Psychiatric Genomics Consortium; International Headache Genetics Consortium; 23andMe Research Team; and Brueggeman, L., et al. (2020). Genetic identification of cell types underlying brain complex traits yields insights into the etiology of Parkinson’s disease. *Nat. Genet.* *52*, 482–493. <https://doi.org/10.1038/s41588-020-0610-9>.
 52. Ren, X., Wen, W., Fan, X., Hou, W., Su, B., Cai, P., Li, J., Liu, Y., Tang, F., Zhang, F., et al. (2021). COVID-19 immune features revealed by a large-scale single-cell transcriptome atlas. *Cell* *184*, 1895–1913.e19. <https://doi.org/10.1016/j.cell.2021.01.053>.

53. Kumari, K., Chainy, G.B.N., and Subudhi, U. (2020). Prospective role of thyroid disorders in monitoring COVID-19 pandemic. *Heliyon* 6, e05712. <https://doi.org/10.1016/j.heliyon.2020.e05712>.
54. Croce, L., Gangemi, D., Ancona, G., Liboà, F., Bendotti, G., Minelli, L., and Chiovato, L. (2021). The cytokine storm and thyroid hormone changes in COVID-19. *J. Endocrinol. Invest.* 44, 891–904. <https://doi.org/10.1007/s40618-021-01506-7>.
55. Sen, A. (2020). Repurposing prolactin as a promising immunomodulator for the treatment of COVID-19: Are common Antiemetics the wonder drug to fight coronavirus? *Med. Hypotheses* 144, 110208. <https://doi.org/10.1016/j.mehy.2020.110208>.
56. Rydzynski Moderbacher, C., Ramirez, S.I., Dan, J.M., Grifoni, A., Hastie, K.M., Weiskopf, D., Belanger, S., Abbott, R.K., Kim, C., Choi, J., et al. (2020). Antigen-Specific Adaptive Immunity to SARS-CoV-2 in Acute COVID-19 and Associations with Age and Disease Severity. *Cell* 183, 996–1012.e19. <https://doi.org/10.1016/j.cell.2020.09.038>.
57. Quiros-Fernandez, I., Poorebrahim, M., Fakhr, E., and Cid-Arregui, A. (2021). Immunogenic T cell epitopes of SARS-CoV-2 are recognized by circulating memory and naïve CD8 T cells of unexposed individuals. *EBio-Medicine* 72, 103610. <https://doi.org/10.1016/j.ebiom.2021.103610>.
58. Nguyen, T.H.O., Rowntree, L.C., Petersen, J., Chua, B.Y., Hensen, L., Kedzierski, L., van de Sandt, C.E., Chaurasia, P., Tan, H.X., Habel, J.R., et al. (2021). CD8(+) T cells specific for an immunodominant SARS-CoV-2 nucleocapsid epitope display high naïve precursor frequency and TCR promiscuity. *Immunity* 54, 1066–1082.e5. <https://doi.org/10.1016/j.immuni.2021.04.009>.
59. Kaech, S.M., and Ahmed, R. (2001). Memory CD8+ T cell differentiation: initial antigen encounter triggers a developmental program in naïve cells. *Nat. Immunol.* 2, 415–422. <https://doi.org/10.1038/87720>.
60. Jergović, M., Coplen, C.P., Uhrlaub, J.L., Besselsen, D.G., Cheng, S., Smithey, M.J., and Nikolich-Zugich, J. (2021). Infection-induced type I interferons critically modulate the homeostasis and function of CD8(+) naïve T cells. *Nat. Commun.* 12, 5303. <https://doi.org/10.1038/s41467-021-25645-w>.
61. Spitzer, S.O., Sitnikov, S., Kamen, Y., Evans, K.A., Kronenberg-Versteeg, D., Dietmann, S., de Faria, O., Jr., Agathou, S., and Káradóttir, R.T. (2019). Oligodendrocyte progenitor cells become regionally diverse and heterogeneous with age. *Neuron* 101, 459–471.e5. <https://doi.org/10.1016/j.neuron.2018.12.020>.
62. Vanzulli, I., Papanikolaou, M., De-La-Rocha, I.C., Pieropan, F., Rivera, A.D., Gomez-Nicola, D., Verkhatsky, A., Rodriguez, J.J., and Butt, A.M. (2020). Disruption of oligodendrocyte progenitor cells is an early sign of pathology in the triple transgenic mouse model of Alzheimer's disease. *Neurobiol. Aging* 94, 130–139. <https://doi.org/10.1016/j.neurobiolaging.2020.05.016>.
63. Agarwal, D., Sandor, C., Volpato, V., Caffrey, T.M., Monzón-Sandoval, J., Bowden, R., Alegre-Abarrategui, J., Wade-Martins, R., and Webber, C. (2020). A single-cell atlas of the human substantia nigra reveals cell-specific pathways associated with neurological disorders. *Nat. Commun.* 11, 4183. <https://doi.org/10.1038/s41467-020-17876-0>.
64. Sims, R., van der Lee, S.J., Naj, A.C., Bellenguez, C., Badarinarayan, N., Jakobsdottir, J., Kunkle, B.W., Boland, A., Raybould, R., Bis, J.C., et al. (2017). Rare coding variants in PLAG2, ABI3, and TREM2 implicate microglial-mediated innate immunity in Alzheimer's disease. *Nat. Genet.* 49, 1373–1384. <https://doi.org/10.1038/ng.3916>.
65. Corces, M.R., Shcherbina, A., Kundu, S., Gloudemans, M.J., Frésard, L., Granja, J.M., Louie, B.H., Eulalio, T., Shams, S., Bagdatli, S.T., et al. (2020). Single-cell epigenomic analyses implicate candidate causal variants at inherited risk loci for Alzheimer's and Parkinson's diseases. *Nat. Genet.* 52, 1158–1168. <https://doi.org/10.1038/s41588-020-00721-x>.
66. Yang, A.C., Vest, R.T., Kern, F., Lee, D.P., Agam, M., Maat, C.A., Losada, P.M., Chen, M.B., Schaum, N., Khoury, N., et al. (2022). A human brain vascular atlas reveals diverse mediators of Alzheimer's risk. *Nature* 603, 885–892. <https://doi.org/10.1038/s41586-021-04369-3>.
67. Xu, J., Zhang, P., Huang, Y., Zhou, Y., Hou, Y., Bekris, L.M., Lathia, J., Chiang, C.-W., Li, L., Pieper, A.A., et al. (2021). Multimodal single-cell/nucleus RNA sequencing data analysis uncovers molecular networks between disease-associated microglia and astrocytes with implications for drug repurposing in Alzheimer's disease. *Genome Res.* 31, 1900–1912. <https://doi.org/10.1101/gr.272484.120>.
68. Sahel, A., Ortiz, F.C., Kerninon, C., Maldonado, P.P., Angulo, M.C., and Nait-Oumesmar, B. (2015). Alteration of synaptic connectivity of oligodendrocyte precursor cells following demyelination. *Front. Cell. Neurosci.* 9, 77. <https://doi.org/10.3389/fncel.2015.00077>.
69. Shang, L., Smith, J.A., and Zhou, X. (2020). Leveraging gene co-expression patterns to infer trait-relevant tissues in genome-wide association studies. *PLoS Genet.* 16, e1008734. <https://doi.org/10.1371/journal.pgen.1008734>.
70. Yao, X., Glessner, J.T., Li, J., Qi, X., Hou, X., Zhu, C., Li, X., March, M.E., Yang, L., Mentch, F.D., et al. (2021). Integrative analysis of genome-wide association studies identifies novel loci associated with neuropsychiatric disorders. *Transl. Psychiatry* 11, 69. <https://doi.org/10.1038/s41398-020-01195-5>.
71. Howard, D.M., Adams, M.J., Clarke, T.-K., Hafferty, J.D., Gibson, J., Shirali, M., Coleman, J.R.I., Hagenaaars, S.P., Ward, J., Wigmore, E.M., et al. (2019). Genome-wide meta-analysis of depression identifies 102 independent variants and highlights the importance of the prefrontal brain regions. *Nat. Neurosci.* 22, 343–352. <https://doi.org/10.1038/s41593-018-0326-7>.
72. Lee, J.J., Wedow, R., Okbay, A., Kong, E., Maghziyan, O., Zacher, M., Nguyen-Viet, T.A., Bowers, P., Sidorenko, J., Karlsson Linnér, R., et al. (2018). Gene discovery and polygenic prediction from a genome-wide association study of educational attainment in 1.1 million individuals. *Nat. Genet.* 50, 1112–1121. <https://doi.org/10.1038/s41588-018-0147-3>.
73. Huang, Y., and Mucke, L. (2012). Alzheimer mechanisms and therapeutic strategies. *Cell* 148, 1204–1222. <https://doi.org/10.1016/j.cell.2012.02.040>.
74. Ochalek, A., Mihalik, B., Avci, H.X., Chandrasekaran, A., Téglási, A., Bock, I., Giudice, M.L., Tancos, Z., Molnár, K., László, L., et al. (2017). Neurons derived from sporadic Alzheimer's disease iPSCs reveal elevated TAU hyperphosphorylation, increased amyloid levels, and GSK3B activation. *Alzheimer's Res. Ther.* 9, 90. <https://doi.org/10.1186/s13195-017-0317-z>.
75. Anderson, A.G., Rogers, B.B., Loupe, J.M., Rodriguez-Nunez, I., Roberts, S.C., White, L.M., Brazell, J.N., Bunney, W.E., Bunney, B.G., Watson, S.J., et al. (2023). Single nucleus multiomics identifies ZEB1 and MAFB as candidate regulators of Alzheimer's disease-specific cis-regulatory elements. *Cell Genom.* 3, 100263. <https://doi.org/10.1016/j.xgen.2023.100263>.
76. Schott, B.H., Wang, L., Zhu, X., Harding, A.T., Ko, E.R., Bourgeois, J.S., Washington, E.J., Burke, T.W., Anderson, J., Bergstrom, E., et al. (2022). Single-cell genome-wide association reveals that a nonsynonymous variant in ERAP1 confers increased susceptibility to influenza virus. *Cell Genom.* 2, 100207. <https://doi.org/10.1016/j.xgen.2022.100207>.
77. Wang, S.K., Nair, S., Li, R., Kraff, K., Pampari, A., Patel, A., Kang, J.B., Luong, C., Kundaje, A., and Chang, H.Y. (2022). Single-cell multiome of the human retina and deep learning nominate causal variants in complex eye diseases. *Cell Genom.* 2, 100164. <https://doi.org/10.1016/j.xgen.2022.100164>.
78. Luo, C., Liu, H., Xie, F., Armand, E.J., Siletti, K., Bakken, T.E., Fang, R., Doyle, W.I., Stuart, T., Hodge, R.D., et al. (2022). Single nucleus multiomics identifies human cortical cell regulatory genome diversity. *Cell Genom.* 2, 100107. <https://doi.org/10.1016/j.xgen.2022.100107>.
79. Garofano, L., Migliozi, S., Oh, Y.T., D'Angelo, F., Najac, R.D., Ko, A., Frangaj, B., Caruso, F.P., Yu, K., Yuan, J., et al. (2021). Pathway-based classification of glioblastoma uncovers a mitochondrial subtype with therapeutic vulnerabilities. *Nat. Cancer* 2, 141–156. <https://doi.org/10.1038/s43018-020-00159-4>.

80. Weiss, T., and Weller, M. (2021). Pathway-based stratification of glioblastoma. *Nat. Rev. Neurol.* *17*, 263–264. <https://doi.org/10.1038/s41582-021-00474-z>.
81. Nasser, J., Bergman, D.T., Fulco, C.P., Guckelberger, P., Doughty, B.R., Patwardhan, T.A., Jones, T.R., Nguyen, T.H., Ullirsch, J.C., Lekschas, F., et al. (2021). Genome-wide enhancer maps link risk variants to disease genes. *Nature* *593*, 238–243. <https://doi.org/10.1038/s41586-021-03446-x>.
82. Dey, K.K., Gazal, S., van de Geijn, B., Kim, S.S., Nasser, J., Engreitz, J.M., and Price, A.L. (2022). SNP-to-gene linking strategies reveal contributions of enhancer-related and candidate master-regulator genes to autoimmune disease. *Cell Genom.* *2*, 100145. <https://doi.org/10.1016/j.xgen.2022.100145>.
83. Han, X., Zhou, Z., Fei, L., Sun, H., Wang, R., Chen, Y., Chen, H., Wang, J., Tang, H., Ge, W., et al. (2020). Construction of a human cell landscape at single-cell level. *Nature* *581*, 303–309. <https://doi.org/10.1038/s41586-020-2157-4>.
84. Zeisel, A., Hochgerner, H., Lönnerberg, P., Johnson, A., Memic, F., van der Zwan, J., Häring, M., Braun, E., Borm, L.E., La Manno, G., et al. (2018). Molecular Architecture of the Mouse Nervous System. *Cell* *174*, 999–1014.e22. <https://doi.org/10.1016/j.cell.2018.06.021>.
85. Grubman, A., Chew, G., Ouyang, J.F., Sun, G., Choo, X.Y., McLean, C., Simmons, R.K., Buckberry, S., Vargas-Landin, D.B., Poppe, D., et al. (2019). A single-cell atlas of entorhinal cortex from individuals with Alzheimer's disease reveals cell-type-specific gene expression regulation. *Nat. Neurosci.* *22*, 2087–2097. <https://doi.org/10.1038/s41593-019-0539-4>.
86. Smith, A.M., Davey, K., Tsartsalis, S., Khozoie, C., Fancy, N., Tang, S.S., Liaptsi, E., Weinert, M., McGarry, A., Muirhead, R.C.J., et al. (2022). Diverse human astrocyte and microglial transcriptional responses to Alzheimer's pathology. *Acta Neuropathol.* *143*, 75–91. <https://doi.org/10.1007/s00401-021-02372-6>.
87. Su, Y., Chen, D., Yuan, D., Lausted, C., Choi, J., Dai, C.L., Voillet, V., Duvvuri, V.R., Scherler, K., Troisch, P., et al. (2020). Multi-Omics Resolves a Sharp Disease-State Shift between Mild and Moderate COVID-19. *Cell* *183*, 1479–1495.e20. <https://doi.org/10.1016/j.cell.2020.10.037>.
88. Sun, T., Song, D., Li, W.V., and Li, J.J. (2021). scDesign2: a transparent simulator that generates high-fidelity single-cell gene expression count data with gene correlations captured. *Genome Biol.* *22*, 163. <https://doi.org/10.1186/s13059-021-02367-2>.
89. Jassal, B., Matthews, L., Viteri, G., Gong, C., Lorente, P., Fabregat, A., Sidiropoulos, K., Cook, J., Gillespie, M., Haw, R., et al. (2020). The reactome pathway knowledgebase. *Nucleic Acids Res.* *48*, D498–d503. <https://doi.org/10.1093/nar/gkz1031>.
90. Liberzon, A., Birger, C., Thorvaldsdóttir, H., Ghandi, M., Mesirov, J.P., and Tamayo, P. (2015). The Molecular Signatures Database (MSigDB) hallmark gene set collection. *Cell Syst.* *1*, 417–425. <https://doi.org/10.1016/j.cels.2015.12.004>.
91. Network and Pathway Analysis Subgroup of Psychiatric Genomics Consortium; Devlin, B., Kelsoe, J.R., Sklar, P., Daly, M.J., O'Donovan, M.C., Craddock, N., Kendler, K.S., A Weiss, L., and Wray, N.R. (2015). Psychiatric genome-wide association study analyses implicate neuronal, immune and histone pathways. *Nat. Neurosci.* *18*, 199–209. <https://doi.org/10.1038/nn.3922>.
92. 1000 Genomes Project Consortium; Auton, A., Brooks, L.D., Durbin, R.M., Garrison, E.P., Kang, H.M., Korbel, J.O., Marchini, J.L., McCarthy, S., McVean, G.A., and Abecasis, G.R. (2015). A global reference for human genetic variation. *Nature* *526*, 68–74. <https://doi.org/10.1038/nature15393>.
93. Kilpinen, H., Goncalves, A., Leha, A., Afzal, V., Alasoo, K., Ashford, S., Bala, S., Bensaddek, D., Casale, F.P., Culley, O.J., et al. (2017). Common genetic variation drives molecular heterogeneity in human iPSCs. *Nature* *546*, 370–375. <https://doi.org/10.1038/nature22403>.
94. Satija, R., Farrell, J.A., Gennert, D., Schier, A.F., and Regev, A. (2015). Spatial reconstruction of single-cell gene expression data. *Nat. Biotechnol.* *33*, 495–502. <https://doi.org/10.1038/nbt.3192>.
95. Yu, F., Sankaran, V.G., and Yuan, G.-C. (2021). CUT&RUNTools 2.0: a pipeline for single-cell and bulk-level CUT&RUN and CUT&Tag data analysis. *Bioinformatics* *38*, 252–254. <https://doi.org/10.1093/bioinformatics/btab507>.
96. Yang, J., Ferreira, T., Morris, A.P., Medland, S.E., Genetic Investigation of ANthropometric Traits GIANT Consortium; DIABetes Genetics Replication And Meta-analysis DIAGRAM Consortium; Madden, P.A.F., Heath, A.C., Martin, N.G., Montgomery, G.W., Weedon, M.N., Loos, R.J., et al. (2012). Conditional and joint multiple-SNP analysis of GWAS summary statistics identifies additional variants influencing complex traits. *Nat. Genet.* *44*, 369–375, S1–S3. <https://doi.org/10.1038/ng.2213>.
97. Tran, D., Nguyen, H., Tran, B., La Vecchia, C., Luu, H.N., and Nguyen, T. (2021). Fast and precise single-cell data analysis using a hierarchical autoencoder. *Nat. Commun.* *12*, 1029. <https://doi.org/10.1038/s41467-021-21312-2>.
98. Stuart, T., Butler, A., Hoffman, P., Hafemeister, C., Papalexi, E., Mauck, W.M., 3rd, Hao, Y., Stoeckius, M., Smibert, P., and Satija, R. (2019). Comprehensive Integration of Single-Cell Data. *Cell* *177*, 1888–1902.e21. <https://doi.org/10.1016/j.cell.2019.05.031>.
99. Goudot, C., Coillard, A., Villani, A.-C., Gueguen, P., Cros, A., Sarkizova, S., Tang-Huau, T.-L., Bohec, M., Baulande, S., Hacohen, N., et al. (2017). Aryl hydrocarbon receptor controls monocyte differentiation into dendritic cells versus macrophages. *Immunity* *47*, 582–596.e6. <https://doi.org/10.1016/j.immuni.2017.08.016>.
100. Monaco, G., Lee, B., Xu, W., Mustafah, S., Hwang, Y.Y., Carré, C., Burdini, N., Visan, L., Ceccarelli, M., Poidinger, M., et al. (2019). RNA-Seq signatures normalized by mRNA abundance allow absolute deconvolution of human immune cell types. *Cell Rep.* *26*, 1627–1640.e7. <https://doi.org/10.1016/j.celrep.2019.01.041>.

STAR★METHODS

KEY RESOURCES TABLE

REAGENT or RESOURCE	SOURCE	IDENTIFIER
Deposited data		
GWAS summary statistics for monocyte count	MRC Integrative Epidemiology Unit (IEU ID: ieu-b-31)	https://gwas.mrcieu.ac.uk/datasets/ieu-b-31/
GWAS summary statistics for lymphocyte count	IEU ID: ebi-a-GCST004627	https://gwas.mrcieu.ac.uk/datasets/ebi-a-GCST004627/
GWAS summary statistics for lymphocyte percent of white cells	IEU ID: ebi-a-GCST004632	https://gwas.mrcieu.ac.uk/datasets/ebi-a-GCST004632/
GWAS summary statistics for mean corpus volume	IEU ID: ebi-a-GCST90002335	https://gwas.mrcieu.ac.uk/datasets/ebi-a-GCST90002335/
GWAS summary statistics for neutrophil count	IEU ID: ieu-b-34	https://gwas.mrcieu.ac.uk/datasets/ieu-b-34/
GWAS summary statistics for white blood cell count	IEU ID: ieu-b-30	https://gwas.mrcieu.ac.uk/datasets/ieu-b-30/
GWAS summary statistics for eosinophil count	IEU ID: ieu-b-33	https://gwas.mrcieu.ac.uk/datasets/ieu-b-33/
GWAS summary statistics for basophil count	IEU ID: ieu-b-29	https://gwas.mrcieu.ac.uk/datasets/ieu-b-29/
GWAS summary statistics for mean corpuscular hemoglobin concentration (MCHC)	IEU ID: ebi-a-GCST90002329	https://gwas.mrcieu.ac.uk/datasets/ebi-a-GCST90002329/
GWAS summary statistics for hemoglobin concentration	IEU ID: ebi-a-GCST90002311	https://gwas.mrcieu.ac.uk/datasets/ebi-a-GCST90002311/
GWAS summary statistics for hospitalized COVID-19	B2_ALL_leave_23andme	https://www.covid19hg.org/
GWAS summary statistics for Alzheimer's disease	IEU ID: ieu-b-2	https://gwas.mrcieu.ac.uk/datasets/ieu-b-2/
Human BMMC-based scRNA-seq data (n = 35,582 cells)	Granjia et al. ⁴⁷	https://jeffgranja.s3.amazonaws.com/MPAL-10x/Supplementary_Data/Healthy-Data/scRNA-Healthy-Hematopoiesis-191120.rds
Human PBMC-based scRNA-seq data (n = 97,039 cells)	Stephenson et al. ⁴⁸	https://www.ebi.ac.uk/arrayexpress/experiments/E-MTAB-10026/
Multiple human organs-based scRNA-seq data (n = 513,707 cells)	Han et al. ⁸³	https://www.ncbi.nlm.nih.gov/geo/query/acc.cgi?acc=GSE134355
Mouse brain-based scRNA-seq data (n = 160,796 cells)	Bryoio et al. ⁸⁴	https://storage.googleapis.com/linnarsson-lab-loom/l5_all.loom
Human brain-based snRNA-seq data (n = 11,768 cells)	Grubman et al. ⁸⁵	https://www.ncbi.nlm.nih.gov/geo/query/acc.cgi?acc=GSE138852
Human brain-based snRNA-seq data (n = 101,906 cells)	Smith et al. ⁸⁶	https://www.ncbi.nlm.nih.gov/geo/query/acc.cgi?acc=GSE160936
Human brain-based snRNA-seq data (n = 14,287 cells)	Agarwal et al. ⁶³	https://www.ncbi.nlm.nih.gov/geo/query/acc.cgi?acc=GSE140231
Human PBMC-based scRNA-seq data (n = 469,453 cells)	Su et al. ⁸⁷	https://www.ebi.ac.uk/arrayexpress/experiments/E-MTAB-9357
Software and algorithms		
R 4.1.3	R Core Team	https://www.r-project.org/
scDesign2 1.0.0	Sun et al. ⁸⁸	https://github.com/JSB-UCLA/scDesign2
KEGG	Kanehisa et al. ⁴²	https://www.genome.jp/kegg/
Seurat 4.3.0	Butler et al. ⁴⁴	https://github.com/satijalab/seurat

(Continued on next page)

Continued

REAGENT or RESOURCE	SOURCE	IDENTIFIER
scDRS 1.0.2	Zhang et al. ²²	https://github.com/martinjzhang/scDRS
LDSC-SEG	Finucane et al. ¹⁶	https://github.com/bulik/ldsc
RolyPoly	Calderon et al. ¹⁸	https://github.com/dcalderon/rolypoly
MAGMA	de Leeuw et al. ²⁶	https://ctg.cncr.nl/software/magma
TWAS	Gusev et al. ²³	https://github.com/gusevlab/fusion_twass
S-PrediXcan	Barbeira et al. ²⁵	https://predictdb.org/
S-MultiXcan	Barbeira et al. ²⁴	https://github.com/hakyimlab/MetaXcan
sc-linker	Jagadeesh et al. ¹⁹	https://github.com/karthikj89/scgenetics
EPIC	Wang et al. ²¹	https://github.com/rujinwang/EPIC

RESOURCE AVAILABILITY

Lead contact

Further information and requests for resources and reagents should be directed to and will be fulfilled by the lead contact, Jianzhong Su (sujz@wmu.edu.cn).

Materials availability

This study did not generate new unique reagents.

Data and code availability

All GWAS summary datasets were downloaded from three publicly accessible databases of the IEU open GWAS project: <https://gwas.mrcieu.ac.uk/>, the COVID-19 Host Genetics Initiative: www.covid19hg.org/results, the Psychiatric Genomics Consortium website: <https://pgc.unc.edu/>, and the NHGRI-EBI GWAS Catalog: <https://www.ebi.ac.uk/gwas/>. The healthy BMMC scRNA-seq dataset was downloaded from a website (https://jeffgranja.s3.amazonaws.com/MPAL-10x/Supplementary_Data/Healthy-Data/scRNA-Healthy-Hematopoiesis-191120.rds). The healthy PBMC scRNA-seq dataset used to validate scPagwas performance was downloaded from the ArrayExpress database (ArrayExpress: <https://www.ebi.ac.uk/arrayexpress/experiments/E-MTAB-10026/>). The mouse brain scRNA-seq dataset was downloaded from the Mouse Brain Atlas (Mouse Brain Atlas: https://storage.googleapis.com/linnarsson-lab-loom/l5_all.loom). Human brain snRNA-seq dataset #1 (GEO: <https://www.ncbi.nlm.nih.gov/geo/query/acc.cgi?acc=GSE138852>), Human brain snRNA-seq dataset #2 (GEO: <https://www.ncbi.nlm.nih.gov/geo/query/acc.cgi?acc=GSE160936>), Human brain snRNA-seq dataset #3 (GEO: <https://www.ncbi.nlm.nih.gov/geo/query/acc.cgi?acc=GSE140231>), and two bulk-based transcriptomic profiles on AD (GEO: 1. <https://www.ncbi.nlm.nih.gov/geo/query/acc.cgi?acc=GSE109887>; 2. <https://www.ncbi.nlm.nih.gov/geo/query/acc.cgi?acc=GSE15222>) were downloaded from the GEO database. The PBMC scRNA-seq dataset on COVID-19 severity was downloaded from the ArrayExpress database (ArrayExpress: <https://www.ebi.ac.uk/arrayexpress/experiments/E-MTAB-9357/>). The scRNA-seq dataset on the human cell landscape (HCL) was downloaded from the GEO database (GEO: <https://www.ncbi.nlm.nih.gov/geo/query/acc.cgi?acc=GSE134355>). scPagwas is implemented as an R package and is available on GitHub (<https://github.com/dengchunyu/scPagwas>). The code to reproduce the results is available in a dedicated GitHub repository (https://github.com/dengchunyu/scPagwas_reproduce) or Zenodo: <https://zenodo.org/record/8137370>.

METHOD DETAILS

scPagwas methodology

The workflow of the scPagwas method is shown in [Figure 1](#). In brief, scPagwas employs an optimized polygenic regression model to identify the associations of a subset of cells with a complex disease or trait of interest. The framework of the method is described in detail in the following steps.

Linking SNPs to their corresponding pathways

Based on previous evidence⁷ indicating that most eQTLs consistently lie in a 20-kb window centered on the transcription start site of a gene, a window size of 20 kb is adopted as the default parameter of scPagwas to assign SNPs from GWAS summary statistics to associated genes. We use the notation $g(k)$ to represent a gene g with an SNP k . With the assignment of SNPs to corresponding gene, there are a few SNPs with multiple associated genes. We duplicate these SNPs and consider them as independent SNP-gene pairs following an earlier study.¹⁸ In our data applications, SNPs with minor allele frequencies smaller than 0.01 or on the sex chromosomes (ChrX-Y) were removed.

Based on pathways in the KEGG database,⁴² we annotate these SNPs to associated gene g in corresponding pathway, and use the notation $S_i = \{k : g(k) \in P_i\}$ to indicate the set of SNPs within the pathway i . The notation P_i indicates the set of genes in the

pathway i . scPagwas provides other functional gene sets, such as Reactome⁸⁹ and MSigDB,⁹⁰ as alternative options. In view of statistics for smaller gene sets were over-dispersed and gene sets with large number of genes were largely non-specific,⁹¹ we limited our analysis to pathways containing 5–300 genes. In our data applications, the 1,000 Genomes Project Phase 3 Panel⁹² was applied to calculate the linkage disequilibrium (LD) among SNPs available in the GWAS summary statistics, and the major histocompatibility complex region (Chr6: 25–35 Mbp)⁹³ was removed because of the extensive LD in this region.

PAS matrix transformation

scPagwas uses the variance-stabilizing transformation method⁹⁴ with a scale factor of 10,000 to normalize a sparse gene-by-cell matrix from scRNA-seq data as follows: $e_{gj} = \log\left(a_{gj} \cdot 1e4 / \sum_g a_{gj} + 1\right)$, where a_{gj} is the raw expression for gene g in cell j and e_{gj} is the normalized expression of gene g in cell j . Pathways such as those from the KEGG database⁴² can be used as a gene set to calculate PASs. The SVD method can greatly improve the computational efficiency^{28,95} of analyzing a sparse matrix with high dimensionality and can be used to generate eigenvalues without calculating the covariance matrix. We apply the SVD method to transform a normalized gene-by-cell matrix into a pathway-by-cell matrix with reduced dimensional space.

For each pathway i , we extract a $N \times M_i$ sub-matrix \mathbf{A}_i from the normalized single-cell matrix \mathbf{A} , with N being the number of cells and M_i being the number of genes in pathway i . Applying the SVD method, \mathbf{A}_i can be decomposed as follows:

$$\mathbf{A}_i^T = \mathbf{U}\mathbf{\Sigma}\mathbf{V}^T,$$

where \mathbf{U} is an $N \times N$ orthogonal matrix, $\mathbf{\Sigma}$ is a diagonal matrix with all zeroes except for the elements on the main diagonal, and \mathbf{V}^T is an $M_i \times M_i$ orthogonal matrix. For the right orthogonal matrix $\mathbf{V} = (\mathbf{v}_1, \mathbf{v}_2, \dots, \mathbf{v}_{M_i})$, the t th column vector \mathbf{v}_t represents the t th principal component. In reference to previous studies,^{34,41} we use the projection of the characteristics of genes in each pathway on the direction of the PC1 eigenvalue to define PAS s_{ij} for the pathway i in cell j , which reflects the main coordinated expression variability of genes in a given pathway among single-cell data.

Polygenic regression model

According to previous methods,^{18,40,96} we assume a linear regression model, $\mathbf{y} = \mathbf{X}\mathbf{b} + \boldsymbol{\varepsilon}$, where \mathbf{y} is an n – vector of phenotypes, \mathbf{X} denotes the $n \times m$ matrix of genotypes (standardized to mean 0 and variance 1 for each SNP vector), \mathbf{b} indicates the per-normalized-genotype effect sizes vector of m SNPs when fitted jointly, and $\boldsymbol{\varepsilon}$ is the stochastic environmental error term. The released GWAS summary dataset contains per-SNP effect estimates, denoted as $\hat{\boldsymbol{\beta}}$. These estimates indicate the marginal regression coefficients from univariate models and can be calculated using the transformation equation $\hat{\boldsymbol{\beta}}_k = \mathbf{X}_k^T \mathbf{y}$, where \mathbf{X}_k^T represents standardized genotypes for SNP k across n GWAS samples. After substituting the polygenic model $\mathbf{y} = \mathbf{X}\mathbf{b} + \boldsymbol{\varepsilon}$ into the estimation equation $\hat{\boldsymbol{\beta}} = \mathbf{X}^T \mathbf{y}$, the estimated marginal effect sizes of SNPs can be written as:

$$\hat{\boldsymbol{\beta}} = \mathbf{R}\mathbf{b} + \mathbf{X}^T \boldsymbol{\varepsilon},$$

where \mathbf{R} denotes the LD matrix.

As previously mentioned, S_i denotes an SNP set that contains SNPs mapped to genes in a pathway i . The polygenic model assumes that the effect sizes of SNPs in pathway i are random effects, which follow the multi-variable normal distribution $\mathbf{b}_{S_i} \sim \text{MVN}(0, \sigma_i^2 \mathbf{I}_{|S_i| \times |S_i|})$, where σ_i^2 is the variance of effect sizes for SNPs in the pathway and \mathbf{I} is the $|S_i| \times |S_i|$ identity matrix. Based on the prior assumption of above polygenic model, the distribution for the vector of the estimated effects of SNPs ($\hat{\boldsymbol{\beta}}_{S_i}$) associated with a pathway follows:

$$\hat{\boldsymbol{\beta}}_{S_i} \sim \text{MVN}\left(0, \sigma_i^2 \mathbf{R}_{S_i} + \sigma_e^2 \mathbf{R}_{S_i}\right)$$

In reference to the extension of stratified LD score regression to continuous annotations,⁴⁰ the per-normalized SNP estimates $\hat{\boldsymbol{\beta}}$ is a mean 0 vector whose variance σ_i^2 depends on continuous-valued annotations (in this case, expression levels of genes in a given pathway). Based on the assumption that a positive correlation between genetic associations and gene expression levels in each cell associated with a trait of interest, the variance σ_i^2 is modeled using the linear weighted sum method for each SNP k :

$$\sigma_i^2 = \tau_0 + \sum_j \tau_{ij} \tilde{e}_{g(k)j}^i,$$

where τ_0 is an intercept term, τ_{ij} is the coefficient for the pathway i in cell j , which measures the strength of association between pathway-specific gene expression activity and the variance of GWAS effect sizes in a given cell, and \tilde{e}_{gj}^i is the adjusted gene expression for each gene g in the given pathway i calculated as $\tilde{e}_{gj}^i = s_{ij} \hat{e}_{gj}$ with s_{ij} being the PAS of pathway i . For each gene g in the pathway i in cell j , to reduce standard deviation and suppress the effect of outliers,⁹⁷ the gene expression e_{gj} is rescaled using the min-max rescaling method:

$$\hat{e}_{gj} = \frac{e_{gj} - \text{MIN}(e_{gj})}{\text{MAX}(e_{gj}) - \text{MIN}(e_{gj})},$$

where $MAX(e_{gj})$ denotes the maximum gene expression in pathway i and $MIN(e_{gj})$ denotes the minimum gene expression in pathway i .

To optimize the coefficients for each pathway in cells under the polygenic regression model, scPagwas adopts the method-of-moments approach, which can prominently improve the computational efficiency and the estimated uniform convergence.¹⁸ Then, the observed and expected squared effects of SNPs relevant to each pathway are fitted, and the following equation is used to estimate the expected value:

$$E(\hat{\beta}_k^2) = \sigma_i^2 (\mathbf{R}_{S_i}^2)_{k,k} + \sigma_e^2,$$

where $(\mathbf{R}_{S_i}^2)_{k,k}$ represents the k th diagonal element of matrix $\mathbf{R}_{S_i}^2$. Then, the coefficient τ_{ij} can be estimated using the following linear regression:

$$E(\hat{\beta}_k^2) = (\mathbf{R}_{S_i}^2)_{k,k} \left(\tau_0 + \sum_j \tau_{ij} \bar{e}_{g(k)j} \right) + \sigma_e^2$$

Of note, the estimated coefficient $\hat{\tau}_{ij}$ represents the per-SNP contribution of one unit of the gene expression activity in the pathway i in cell j to heritability. We define a gPAS for each pathway i in a cell j that is calculated by the product between the estimated coefficient $\hat{\tau}_{ij}$ and weighted PAS within a given cell using the following equation: $gPAS_{ij} = \hat{\tau}_{ij} \sum_{g \in P_i} \frac{e_{gj}}{M_i} s_{ij}$, where M_i is the number of genes in the pathway i , and s_{ij} is the PAS for the pathway i in cell j . Essentially, gPAS is a pathway-activity-based prediction of the genetic variance of a normal distribution of cis-GWAS effect sizes for each pathway in a given cell (Figure 1D), and these cell-specific gPASs can be used to rank trait-relevant pathways (see Methods S2). The total genetic variance explained by all pathways in a given cell is calculated by summing all the metrics of gPASs in the cell: $gPAS_j^{sum} = \sum_{i=1}^K gPAS_{ij}$, where K is the total number of pathways in cell j . Note that the larger summed gPASs ($gPAS^{sum}$) for each cell would have larger contribution to the heritability of a trait.

Identification of trait-relevant genes and individual cells

To optimize genes relevant to complex diseases/traits at single-cell resolution, we determine which gene g exhibits expression that is highly correlated with the summed gPASs ($gPAS^{sum}$) across individual cells using the Pearson correlation method. To maximize the power, the expression of each gene g is inversely weighted by its gene-specific technical noise level, which is estimated by modeling the mean-variance relationship across genes in the scRNA-seq data.⁹⁸ By arranging the PCCs for all genes in descending order, we select the top-ranked risk genes as trait-relevant genes (default top 1,000 genes) according to a previous method.²²

Subsequently, we quantify the aggregate expression of predefined trait-relevant genes in each cell to generate raw TRSs. For a given cell j and a trait-relevant gene set B , the cell-level raw TRS, TRS_j , is defined as the average relative expression of the genes in B . However, such raw TRSs may be confounded by cell complexity, as cells with higher complexity would have more genes identified and consequently tend to have higher TRSs for any given gene set. To properly control for the effect of cell complexity, we calculate a control cell score with a control gene set B^{ctrl} , which is randomly selected in a manner that maintain a comparable distribution of expression levels to that of the predefined gene set. The process included two steps: 1) using the average expression levels to group all analyzed genes into 25 bins of equal size and 2) randomly selecting 100 genes from the same expression bin for each gene in the predefined gene set. The final TRS is defined as the initial raw TRS after subtracting its corresponding control cell score: $\widehat{TRS}_j = \sum_{g \in B} e_{gj} / |B| - \sum_{g \in B^{ctrl}} e_{gj} / |B^{ctrl}|$. The *AddModuleScore* cell-scoring method in Seurat⁴⁴ is employed to calculate the TRS with default parameters.

To further assess whether a cell is significantly associated with the trait of interest, we employ a MC method²² to determine the statistical significance of individual cells by comparing the scPagwas TRS to the empirical distribution of control TRSs for each cell. Initially, let T be a test statistic calculated from the scPagwas TRS of the given set of cells. Second, we sample C control gene sets from a given cell j , which match mean expression and expression variance of top trait-relevant genes. By using the *AddModuleScore* function in Seurat, we use the expression of 1,000 control genes in each gene set to calculate the control TRS for each gene set (denoted as T^{ctrl}) in cell j . Let $T_1^{ctrl}, \dots, T_C^{ctrl}$ be the same test statistics calculated from the C sets of control TRSs of the same set of cells. The MC P value for each cell j can be written as:

$$P_j^{MC} = \frac{1 + \sum_{c=1}^C \mathbb{1}(T_j < T_c^{ctrl})}{1 + C}$$

To enhance the computing speed of scPagwas, the number of sampled control gene sets is set to be 500 in default. As alternative options, users can choose the number of 100 or 1,000 control gene sets for specific purpose.

Note that the running of scPagwas is computationally efficient and scales linearly with the increased number of cells for both computational cost and random access memory (RAM) use. The increased number of SNPs would take more computational cost, whereas not demand the largely increased RAM memory use. It takes 20 minutes and 20 Gb RAM memory to analyze

25,000 cells and one million SNPs, and takes 75 minutes with the requirement of 70 Gb RAM memory to analyze 100,000 cells and one million SNPs (Figure S7).

Inference analysis of trait-relevant cell types

scPagwas can also identify trait-relevant cell types, where the set of cells is treated as a pseudo-bulk transcriptomic profile and the expression of a gene across cells is averaged within a given cell type. For the cell type association, the block bootstrap method⁴⁵ is used to estimate the standard error and compute a t-statistic with a corresponding P value for each cell type. Because the goal of the block bootstrap is to maintain data structures when sampling from the empirical distribution, we leverage all pathways in the KEGG database⁴² to partition the genome into multiple biologically-meaningful blocks and sample these pathway-based blocks with replacement. Under default parameters, scPagwas performs 200 block bootstrap iterations for each cell-type association analysis. The optional parameters are provided for the block bootstrap. Detailed information on scPagwas cell type-level inference analysis can be found in the Methods S1.

Simulations

We used scDesign2 (version 1.0.0)⁸⁸ to simulate a ground truth scRNA-seq dataset containing five cell types including monocytes, DCs, and B, NK, and T cells to assess the performance of scPagwas in identifying monocyte count trait-relevant individual cells. DC, a type of cell differentiated from monocytes,⁹⁹ was chosen as a non-trait-relevant cell type, which could be a confounding factor for distinguishing monocytes from all simulated cells. In the model-fitting step, we first fitted a multivariate generative model to a real dataset via the fluorescence-activated cell-sorted bulk hematopoietic populations downloaded from the GEO database (Accession No. GSE107011).¹⁰⁰ Because there were five sorted cell types, we divided the datasets into five subsets according to the cell types and fitted a cell type-specific model to each subset. In the data-generation step, we generated a synthetic scRNA-seq dataset from the fitted model to represent trait-relevant cell populations (monocytes) and non-trait-relevant cell populations (non-monocyte cells including DCs and B, NK, and T cells) for the monocyte count trait. Finally, we obtained 2,000 cells with synthetic scRNA-seq data with cell proportions of 0.5 (monocytes), 0.05 (DCs), 0.2 (B cells), 0.05 (NK cells), and 0.2 (T cells).

scRNA-seq datasets

Eight independent scRNA-seq or snRNA-seq datasets spanning 1.4 million human (*Homo sapiens*) and mouse (*Mus musculus*) cells were used in this study (Table S1). For blood cell traits, we collected two scRNA-seq datasets based on human BMDCs (n = 35,582 cells)⁴⁷ and human PBMCs (PBMC #1, n = 97,039 cells)⁴⁸ to identify trait-relevant cell subpopulations or types. For AD, we collected four single-cell datasets including a mouse brain scRNA-seq dataset (n = 160,796 cells),⁸⁴ a human brain entorhinal cortex snRNA-seq dataset (Human brain #1, n = 11,786 cells),⁸⁵ a human brain snRNA-seq dataset (Human brain #2, n = 101,906 cells),⁸⁶ and another human brain snRNA-seq dataset (Human brain #3, n = 14,287 cells).⁶³ To identify severe COVID-19-related immune cell populations, we collected a large-scale PBMC scRNA-seq dataset (PBMC #2, n = 469,453 cells) containing 254 peripheral blood samples from patients with various COVID-19 severities (mild N = 109 samples, moderate N = 102 samples, and severe N = 50 samples) and 16 healthy controls.⁸⁷ The scRNA-seq dataset from the human cell landscape (HCL, n = 513,707 cells in 35 adult tissues),⁸³ as well as the previously mentioned four scRNA-seq datasets (i.e., BMDC, PBMC #1, Human brain #1, and Mouse brain), were used to assess the performance of scPagwas in reducing the sparsity and technical noise.

GWAS summary datasets for complex diseases and traits

We obtained GWAS summary statistics for 10 blood cell traits (average N = 307,772) and AD (21,982 cases and 41,944 controls) from the IEU OpenGWAS, for schizophrenia (67,390 cases and 94,015 controls) from the Psychiatric Genomics Consortium, and for severe COVID-19 (7,885 cases and 961,804 controls) from the COVID-19 Host Genetics Initiative (Table S2). The 10 blood cell traits included monocyte count, lymphocyte count, lymphocyte percent, mean corpus volume, neutrophil count, white blood count, eosinophil count, basophil count, mean corpuscular hemoglobin, and hemoglobin concentration.

QUANTIFICATION AND STATISTICAL ANALYSIS

For benchmarking analyses, we evaluated the performance of scPagwas for identifying trait-relevant genes compared with four gene-scoring methods, including MAGMA,²⁶ TWAS,²³ S-PrediXcan,²⁵ and S-MultiXcan,²⁴ and assessed the cell-type-level performance of scPagwas compared with five cell-type inference methods, including sc-linker⁹ and EPIC,²¹ LDSC-SEG,¹⁶ MAGMA-based approach,⁵¹ and RolyPoly.¹⁸ We also used four cell-scoring methods, including *AddModuleScore* function in Seurat,⁴⁴ scDRS,²² AU-Cell,³³ and VISION,³⁵ to evaluate the performance of scPagwas at the single-cell level. The two-sided Student's t test was used to assess the significant differences in gene expressions between Alzheimer's disease (AD) patients and matched controls in two bulk-based transcriptomic datasets (GSE15222, n = 363; GSE109887, n = 78). In reference to a previous study,²¹ we applied the RISmed method⁶⁹ to search supporting evidence for the relationship between interested key words (i.e., the link between scPagwas-identified risk genes and AD from reported studies in the PubMed database).